Continuously Tunable Spintronic Emission in the sub-THz Range

I. Ilyakov[1], N. Awari[1, 2], S. Kovalev[1], C. Fowley[1], K. Rode[3], Y.-C. Lau[3], D. Betto[3], N. Thiyagarajah[3], B. Green[1], O. Yildrim[1], J. Lindner[1], J. Fassbender[1], M. Coey[3], A. Deac[1], M. Gensch[1]

[1]HZDR, Bautzner Landstr. 400, 01328 Dresden, Germany, i.ilyakov@hzdr.de
[2]University of Groningen, 9747 AG Groningen, Netherlands
[3]CRANN, AMBER and School of Physics, Trinity College Dublin, Dublin 2, Ireland

Terahertz (THz) emission spectroscopy is a widely used precise technique giving the ability of studying various processes on subpicosecond time scale. It is based on excitation (typically by femtosecond laser pulses) of non-equilibrium processes in studied media by intense ultrashort photon pulses and further detection of emitted THz light emitted. Typically, the emitted pulses are very broadband single-cycle THz transients and the emission spectrum is governed by the laser pulse duration, carrier relaxation time, phonon absorption, and/or the electro-optical coefficients [1].

In 2004, it was discovered that in the case of magnetized materials the emitted single-cycle THz radiation contains information about the demagnetization process driven by the laser pulses [2, 3]. Then, the THz emission spectroscopy was successfully applied to determine the duration of ultra-fast laser-driven spin currents [4]. Most recently, two groups have succeeded in detecting narrow-band emission from spin waves in ferromagnetic bulk insulators [5, 6].

In this work, we demonstrate the ability of THz emission spectroscopy for characterization of ultra-thin $Mn_{3-x}Ga$ ferromagnetic films. These films have recently attracted considerable attention due to their unique combination of low saturation magnetization, high spin polarization, high magneto-crystalline anisotropy, and low magnetic damping. In $Mn_{3-x}Ga$, these properties are easily tuned by varying the Mn content, which modifies the center frequency of the magnetization precession. This makes $Mn_{3-x}Ga$ thin films interesting candidates for free layers in spin-transfer-torque driven oscillators [7, 8]. Typically, these films are very thin, from tens to sub-ten nm thicknesses and the ways of characterization of these materials are under current research.

The studied samples with 10-65 nm thicknesses were irradiated by femtosecond laser pulses at normal incidence [9]. A small external magnetic field (100-400 mT) was applied in the plane of the sample in order to synchronize the precession of the spins after the ultra-fast laser heating allowing for the emission of a coherent THz wave. The precession frequency is one of the key parameters in spin-transfer-torque oscillators, which determines the working frequency of the device. This frequency is determined by the next formula

$$f_{res}=(\gamma_{eff}/2\pi)(\mu_0 H_k-\mu_0 M_s) \quad (1)$$

where γ_{eff} is an effective value of the gyromagnetic ratio, $\mu_0 H_k$ is an effective perpendicular anisotropy field. M_s is the net saturation magnetization. The saturation magnetization was measured by vibrating sample magnetometry. However, the magnetic anisotropy field, $\mu_0 H_k$, had a very high value which exceeds the field available in our magnetometer. So it was not possible to saturate the magnetization in the plane of the films. However, this parameter can be also determined from the precession frequency.

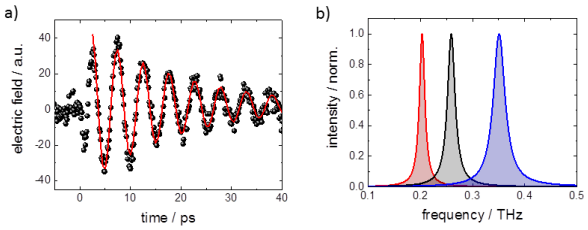

Fig.1. Analysis of the THz emission measurements a) example: sequential electro-optic sampling of an emitted THz transient from Mn_2Ga taken with time steps of 130 fs (bullets). A damped sin function is fitted to derive the center frequency (red solid). b) Fourier transformation of the fits to the electro-optic sampling measurements yields an approximation of the natural line-width. Shown in the plot are the thereby derived spectra for Mn_2Ga (red-left), $Mn_{2.5}Ga$ (black-center) and Mn_3Ga (blue-right).

The emitted radiation was measured by THz time-domain electrooptic sampling. The central frequency of the measured emission lies in a frequency range between 0.15THz and 0.52THz, and can be continuously tuned by Mn content, temperature and external magnetic field. The measured frequencies corresponds to the value of $\mu_0 H_k$ in the range from roughly 8 T for Mn_2Ga to 13 T for Mn_3Ga that is in good agreement with literature values [10,11]. These values were calculated using Eq. (1), M_s and f_{res}. Furthermore, the emission field amplitude per nm thickness for their narrow frequency band was up to an order higher than for 100mkm ZnTe crystal. Thus, optimization of the emitter geometry or the use of multi-layer stacks of nanofilms would potentially increase the output power.

Our results demonstrate that the THz emission spectroscopy is a competitive technique to measure magnetic properties of ultra-thin films. The precession frequency of the $Mn_{3-x}Ga$ films lies in the sub-THz frequency band that confirms its applicability of using in spin-torque devices. The efficiency of the spintronic emission is, within the narrow emission bandwidth, much higher than that of classical ZnTe emitters based on optical rectification. At this moment the study of the sub-10 nm thick samples is under current research and these results will be also performed in the presentation.

Acknowledgment. The authors acknowledge support from the European Commission's Horizon 2020 research and innovation programme under grant agreement No. DLV-737038 (TRANSPIRE).

References

1. X. C. Zhang, X. C. Zhang, B. B. Hu, J. T. Darrow, and D. H. Auston, "Generation and femtosecond electromagnetic pulses from semiconductor surfaces," Appl. Phys. Lett. 56, 1011 (1990).

2. E. Beaurepaire, G. M. Turner, S. M. Harrel, M. C. Beard, J.-Y. Bigot, and C. A. Schmuttenmaer, "Coherent terahertz emission from ferromagnetic films excited by femtosecond laser pulses," Appl. Phys. Lett. 84, 3465 (2004).

3. D. J. Hilton, R. D. Averitt, C. A. Meserole, G. L. Fisher, D. J. Funk, J. D. Thompson, and A. J. Taylor, "Terahertz emission via ultrashort-pulse excitation of magnetic metal films," Opt. Lett. 29, 1805 (2004).

4. T. Kampfrath, M. Battiato, P. Maldonado, G. Eilers, J. Notzold, S. Mahrlein, V. Zbarsky, F. Freimuth, Y. Mokrousov, and S. Blugel, "Terahertz spin current pulses controlled by magnetic heterostructures," Nat. Nano. 8, 256 (2013).

5. T. H. Kim, S. Y. Hamh, J. W. Ham, C. Kang, C.-S. Kee, S. Jung, J. Park, Y. Tokunaga, Y. Tokura, and J. S. Lee, "Coherently controlled spin precession in canted antiferromagnetic YFeO3 using terahertz magnetic field," Appl. Phys. Exp. 7, 093007 (2014).

6. Z. Jin, Z. Mics, G. Ma, Z. Cheng, M. Bonn, and D. Turchinovich, "Singlepulse terahertz coherent control of spin resonance in the canted antiferromagnet YFeO3, mediated by dielectric anisotropy," Phys. Rev. B 87, 094422 (2013).

7. M. Zic, K. Rode, N. Thiyagarajah, Y.-C. Lau, D. Betto, J. M. D. Coey, S. Sanvito, K. J. O'Shea, C. A. Ferguson, and D. A. MacLaren, "Designing a fully compensated half-metallic ferrimagnet," Phys. Rev. B 93, 140202(R) (2016).

8. K. Borisov, D. Betto, Y.-C. Lau, C. Fowley, A. Titova, N. Thiyagarajah, G. Atcheson, J. Lindner, A. M. Deac, J. M. D. Coey et al., "Tunnelling magnetoresistance of the half-metallic compensated ferrimagnet Mn2RuxGa," Appl. Phys. Lett. 108, 192407 (2016).

9. N. Awari, S. Kovalev, C. Fowley, K. Rode, R. A. Gallardo, Y.-C. Lau, D. Betto, N. Thiyagarajah, B. Green, O. Yildirim, J. Lindner, J. Fassbender, J. M. D. Coey, A. M. Deac, and M. Gensch, Narrow-band tunable terahertz emission from ferrimagnetic Mn3-xGa thin films, Appl. Phys. Lett. 109, 032403 (2016).

10. H. Kurt, K. Rode, M. Venkatesan, P. Stamenov, and J. M. D. Coey, "High spin polarization in epitaxial films of ferrimagnetic Mn3Ga," Phys. Rev. B 83, 020405 (2011).

11. H. Kurt, K. Rode, M. Venkatesan, P. Stamenov, and J. M. D. Coey, "Mn3 xGa ($0 \leq x \leq 1$): Multifunctional thin film materials for spintronics and magnetic recording," Phys. Status Solidi B 248, 2338 (2011).

Frequency comb for THz metrology and spectroscopy

C. Bray[1], A. Cuisset[1], F. Hindle[1], JF. Lampin[2] and G. Mouret[1]

[1] Laboratoire de Physico-Chimie de l'Atmosphère, Université du Littoral Côte d'Opale, 189A Avenue Maurice Schumann, 59140 Dunkerque, France, mouret@univ-littoral.fr

[2] Institute of Electronics, Microelectronics and Nanotechnology, UMR 8520, University of Lille, Villeneuve d'Ascq, France

Frequency combs (FC) have radically changed the landscape of frequency metrology and high-resolution spectroscopy investigations extending tremendously the achievable resolution while increasing signal to noise ratio. By describing two experiments, we highlight that like other spectral ranges, THz domain can exploit a frequency comb.

First, the photomixing experiment we have developed at the LPCA during the last decade is presented on figure 1. This spectrometer is able to work between 300 and 3000 GHz with a frequency accuracy and a THz frequency linewidth suitable for high resolution THz spectroscopy [1-2]. The photomixing process is known from long time, and consist to convert an optical beat note into the THz domains. It is one of the best approach to cover a large part of the THz frequency gap. Thus, the frequency of the THz radiation produced is just the difference frequency of the two lasers working around 750 nm (and corresponding to a frequency around 400 THz) required to use of photomixer made in LTG GaAs. In principle, the frequency accuracy of the radiated THz radiation depends of the frequency accuracy of the pumps lasers. Clearly, there are no commercial solution to reach a precision better than 100 kHz often required for high resolution rotational spectroscopy. An alternative way consists to use a FC produce by a femtosecond laser as a ruler to control and to measure the difference frequency between the two pump lasers. In the present demonstration, the FC is produced by a frequency doubled erbium doped modelocked fiber laser with a stabilized repetition rate around 100 MHz. A beatnote between the laser and the nearest FC mode was isolated and phase locked to a local oscillator coherently locking the diode to the FC. The locking of the second laser to a different FC mode allows the difference frequency between the pump lasers to be synthesized. Feedback correction signal is applied to control the difference frequency of pump laser, and thus the THz frequency. The difference of frequency between the diode lasers can be expressed in Eq. (1) as:

$$f_{THz} = n \cdot f_{rr} \pm f_s \pm f_s \quad (1)$$

where f_{rr} is the repetition rate of the femtosecond laser, n is an integer, and f_s is the frequency of the synthesizer used to phase lock the beat signals against synthesizer to a precise frequency control. A classical commercial wavemeter is used to remove the ambiguity of the integer.

Various species have been study by use of this spectrometer from highly polar molecules (OCS, H_2CO) up to low and non-polar (CH_3D, CH_4) compounds and as well as radicals (OH, SO) to cite a fews [3-6].

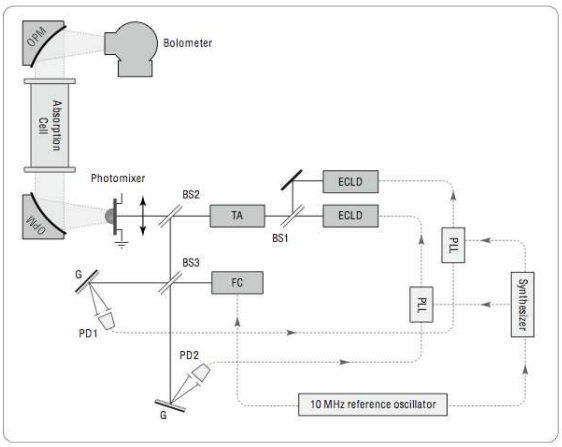

Fig. 1. Experimental setup of the THz photomixing spectrometer. BS1 is a beam splitter to overlap the two laser beams from the two External Cavity Diode Laser (ECDL) and seed Tapered Amplifier (TA). Then, the optical beat note is divided by a second beam splitter (BS2) to produce THz radiation and to manage the THz frequency. BS3 is used to overlap optical beat note and the frequency comb. Two grating (G) disperse the FC and the two lasers to ensure a heterodyne analysis between each ECDL and a part of FC thank to photodiodes (PD1 and PD2). The heterodyne signals are used to control the frequency of each laser.

Second, a very popular approach for THz investigations is the well-known THz Time Domain Spectrometer. Except the dual comb approach, the discrete spectral properties of the generated radiation which forms a THz offset free frequency comb is often ignored. However, the exploitation of the frequency comb structure of THz pulses should lead to an exceptional frequency resolution. To explore this approach, a dedicated heterodyne detection has been implemented around 200 GHz in order to analyse at very high resolution the THz FC (figure 2). Knowing exactly the repetition rate of the femtosecond laser used to produce the THz FC and intermediate frequency thanks to spectrum analyser, different components of the THz FC can be identified without ambiguity (figure 3). By tuning the repetition rate and/or the frequency of the local oscillator, high resolution spectroscopy can be performed [7].

Those two examples show the potential of the Frequency Comb to improve spectroscopic investigations in the THz domain.

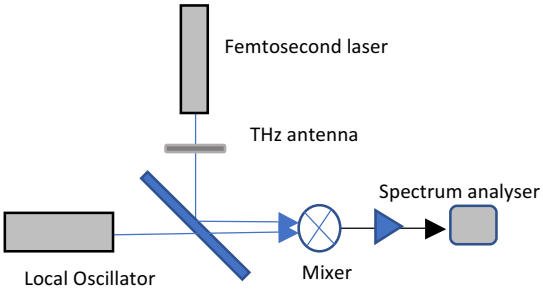

Fig. 2. Heterodyne spectrometer. The THz FC is produced by focusing optical fs pulses onto a a photoconductive dipole antenna. The THz FC and the local oscillator (formed by an amplifier multiplier chain driven by a synthesizer) is overlapped by a beam splitter to feed a subharmonic mixer. After amplification, the intermediate frequency (IF) signal is recorded by a classical spectrum analyzer.

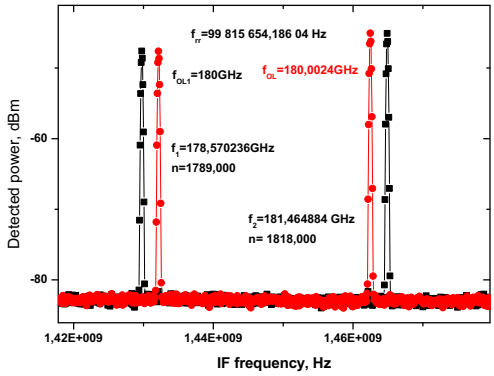

Fig. 3. High resolution spectra of the THZ FC obtained by use of heterodyne detection in which each component is clearly identified by an integer corresponding to an exact harmonic of the repetition rate.

Acknowledgements

This study was undertaken as part of the HEROES project which is financially supported by Agence Nationale pour la Recherche (project number ANR-16-CE30-0020).

References

1. *G. Mouret, et al.,* THz photomixing synthesizer based on a fiber frequency comb // Optics Express, Vol. 17(24), 22031-22040 (2009)

2. *F. Hindle, et al.,* Widely tunable THz synthesizer // Applied Physics B Vol. 104(4) 763-768 (2011)

3. *S. Eliet, et al.*, Rotational spectrum of formaldehyde reinvestigated using a photomixing THz synthesizer // Journal of Molecular Spectroscopy, Vol. 279, 12-15 (2012)

4. *M.A. Martin-Drumel, et al.,* New investigation on THz spectra of OH and SH radicals // Chemical Physics Letters, Vol. 550, 8 – 14 (2012)

5. *C. Bray, et al.,* CH_3D photomixing spectroscopy up to 2.5 THz: New set of rotational and dipole parameters, first THz self-broadening measurements // Journal of Quantitative Spectroscopy & Radiative Transfer, Vol. 189, 198-205 (2017)

6. *C. Bray, et al.* Spectral lines of methane measured up to 2.6 THz at sub-MHz accuracy with a CW-THz photomixing spectrometer: Line positions of rotational transitions induced by centrifugal distortion // *Journal of Quantitative Spectroscopy & Radiative Transfer, Vol. 203, 349-354 (2017).*

7. *S. Skryl et al.,* High-resolution terahertz spectroscopy with a single tunable frequency comb //Opt. Optics Express, Vol. 22 (26), 32276-32281 (2014).

Terahertz lasers based on donor intracenter transitions in silicon

V.N. Shastin[1]

[1]Institute for Physics of Microstructures, Nizhniy Novgorod, Russia, shastin@ipmras

This talk presents a brief overview of terahertz (THz) lasing which is based on the intracenter transitions of impurity Coulomb centers in semiconductors. By now such kind of effects is obtained on group-V donor centers (phosphor P, antimony Sb, arsenic As, bismuth Bi). Energy diagram group-V donor states is shown on Fig.1.

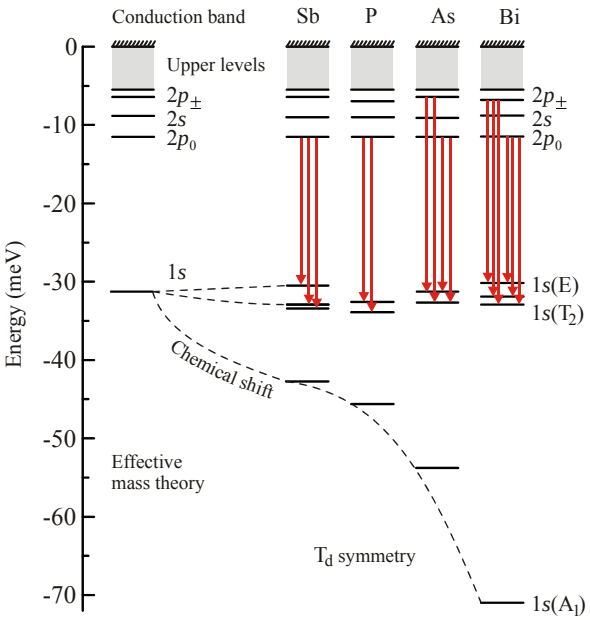

Fig. 1. Energy diagram group-V donor states in silicon. Arrows show possible "normal" laser transitions.

Depending on the pump parameters (frequency, intensity) one can reach either "normal" laser action which develops due to the population inversion between localized donor states or inversionless Raman lasing. Normal lasing occur under optical pumping by a midinfrared laser (for instance by a CO_2 laser) emitting at discrete lines originated from the $2p_0 \rightarrow 1s(T_2)$ and the $2p_\pm \rightarrow 1s(E,T_2)$ transitions subsequently from P, Sb and As, Bi centers in the wavelength range 4,5 – 6,4 THz [1]. Needed population of pointed states are controlled by phonon-assisted relaxation for cryogenic temperatures ($T < 20$ K). Under the same conditions and an intracenter optical excitation of donors one can obtain additionally Raman THz lasing on the transitions between so called "virtual" and 1s(E) final states. As shown the frequency of Raman lasing can be continuously changed between 4,5 – 6,4 THz varying the pump frequency. Normal and Raman lasing of donors were studied using free electron laser FELIX (Netherlands) facility.

Last years the experimental and theoretical activity was focused on the investigation of group-V donor lasing from axially strained silicon crystals. It has been shown that even moderate compressive stress applied along the [100] axis brings to a significant change of THz laser performance of group-V donors [1,2]. There is an optimal strain which may considerably reduce (up to two orders of magnitude) the laser threshold pump intensity increasing small signal gain and efficiency if it concerns normal lasing (see Table1).

Characteristics	Zero stress	Stress along [100] direction
Gain:		
Photo ionization (10,6 μm)	≤ 0,2 cm^{-1}	*1 cm^{-1}
Intracenter pumping (36 μm)	2–4 cm^{-1}	–
Quantum efficiency:		
Photo ionization (10,6 μm)	*≤1%	*≤10%
Photo ionization (17 μm)	–	*≤15%
Intracenter pumping (19–39 μm)	* 50%	–
Efficiency (10,6 μm):	*up to 10^{-3}	*up to 10^{-2}
Pump threshold (10,6 μm):	≥ 15 – 100 kW/cm^2	≥ 100 – 200 W/cm^2
Frequency tuning:	Absence	Δω/ω~1%
Operating temperature:	< 15 – 30 K	
Donor concentration:	$(2 – 4)\times10^{15}$ cm^{-3}	
Frequency range:	5,4 – 6,4 THz	

Tab. 1. Characteristics of "normal" THz silicon lasers; * – theoretical estimate.

It is clear that a value of the optimal strain depends on the doping agent. The influence of the axial strain on Raman lasing is still under continuation. The possible mechanisms behind the strain of the host crystal will be discussed.

In conclusion it is worth to touch the issue of another donor centers in the context of THz lasing from silicon.

References

1. *Pavlov, S.G., Zhukavin, R.Kh., Shastin, V.N., Hübers, H.-W.* The Physical principles of terahertz silicon lasers based on intracenter transitions // Physica Status Solidi B. 2013. V.250. P.9-36.

2. *Kovalevsky, K.A., Abrosimov, N.V., Zhukavin, R.Kh., Pavlov, S.G., Hübers, H.-W., Tsyplenkov, V.V., Shastin, V.N.* Terahertz lasers based on intracentre transitions of group V donors in uniaxially deformed silicon // Quantum Electronics. 2015. V.45 (2). P.113–120.

THz stimulated emission at interband transitions in HgTe/CdHgTe quantum wells

V.I.Gavrilenko[1], V.V.Rumyantsev[1], A.A.Dubinov[1], S.V.Morozov[1], N.N.Mikhailov[2], S.A.Dvoretsky[2], F.Teppe[3], C.Sirtori[4]

[1]Institute for Physics of Microstructures, Nizhny Novgorod, Russia, gavr@ipmras.ru
[2]A.V.Rzhanov Institute of Semiconductor Physics, Siberian Branch of Russian Academy of Sciences, Novosibirsk, Russia
[3]Charles Coulomb Laboratory, University of Montpellier & CNRS, Montpellier, France
[4]Laboratory of Materials and Quantum Phenomena, University Paris-Diderot, Paris, France

Terahertz (THz) spectral range still lacks compact and efficient radiation sources. Quantum cascade lasers (QCLs) based on GaAs and InP demonstrate remarkable performance in the spectral range from 1 THz to 5THz and above 15 THz[1] the "gap" resulting from strong two-phonon absorption. The interband lasers are a straightforward alternative, but in narrow-gap materials the non-radiative Auger recombination is expected to be very effective. Lead salt diode lasers are known to operate up to 50 μm[2]. (though their figures of merit are very limited). The factor that mitigates the Auger recombination in PbSnSe is the symmetry between electron and hole dispersion laws. For energy and momentum conservation laws to be fulfilled, the summarized kinetic energy of the three particles involved in the Auger process has to be over a certain threshold energy E_{th}[3] that decreases if there are heavy mass carries, e.g. heavy holes.

Symmetric energy-momentum laws are realized in HgTe/CdTe based quantum wells (QWs). In HgCdTe QW structures with bandgap 60 - 80 meV we observed the increase of carrier lifetimes with the pumping intensity up to several microseconds due to saturation of Shockley-Read-Hall (SRH) recombination centers, inferring that optical gain can be obtained under reasonable pumping intensity[4]. Earlier the longest wavelength of 5.3 μm was obtained in HgCdTe-based lasers that did not exploit QWs in its design[5]. In this work, we report stimulated emission (SE) from HgCdTe structures at wavelengths up to λ ~ 20 μm, and demonstrate possibilities for HgCdTe based lasers to enter 5 – 15 THz frequency domain.

Structures under study were grown by molecular beam epitaxy on semi-insulating GaAs(013)[6]. Energy spectra were calculated in the framework of Kane 8x8 model. Structure #1 contains ten 12 nm thick $Hg_{0.87}Cd_{0.13}Te/Cd_{0.65}Hg_{0.35}Te$ QWs and structure #2 - five 5.4 nm thick $Hg_{0.91}Cd_{0.09}Te/Cd_{0.6}Hg_{0.4}Te$ QWs. The structures were designed so as to effectively confine light to in-plane direction, therefore the "active" region (5 - 12 QWs) was placed at the antinode position of TE_0 mode in a thick (several micrometers) dielectric waveguide. Due to a quite specific growth direction (013), naturally cleaved facets do not form the Fabri-Perot resonator. Thus, the stimulated emission (SE) studied in this work results from single-pass amplification.

SE spectra for two samples under study at 8K and a "critical" temperature T_{max}, above which no SE is observed, are given in Fig. 1. The emission intensity demonstrates clear threshold dependence on pumping power, typical for the onset of SE. Another telltale sign of the SE is photoluminescence (PL) line narrowing.

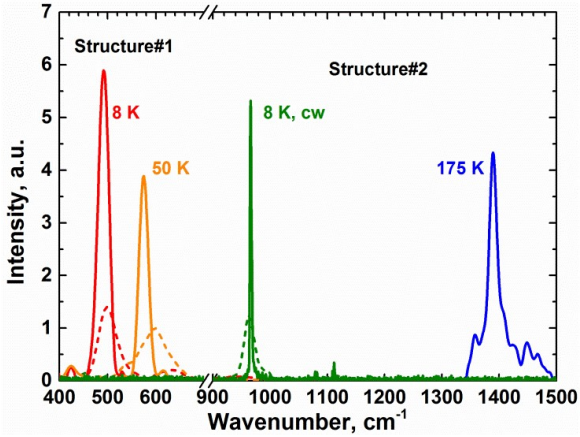

Fig. 1. SE spectra at different temperatures (solid curves) obtained under pulsed pumping with 2.3 μm wavelength and 10 kW/cm^2 intensity for Structure #1 (at both temperatures) and 65 kW/cm^2 for Structure #2 at 175K. SE for Structure #2 at T = 8K was obtained at cw excitation with 0.9 μm wavelength 7 W/cm^2 intensity. Dash curves show PL spectra obtained with the same cw pumping source at 5 W/cm^2 intensity for Structure #1 and 1 W/cm^2 for Structure #2 at 8 K.

The corresponding thresholds are 5 kW/cm^2 and 120 W/cm^2 for SE wavelength ~20 μm (15 THz) and ~10 μm (30 THz) at low temperatures. However, these values are obtained for "below barrier" excitation ($\hbar\omega < E_g$ in barriers), i.e. when non-equilibrium carriers are generated in QWs only. Taking for estimation the QW absorption as 1% one can find the corresponding carrier density in each QW $n_{th} = 1.4\times10^{11}$ cm^{-2} for λ_p = 2.3 μm and I_{th} = 0.12 kW/cm^2 pumping intensity. This n_{th} value agrees fairly well with our previous calculations[7]. It also allows estimating the equivalent threshold current density for 5 QWs placed into a *p-n* junction as $j_{th} = 5en_{th}/\tau_{pulse}$ (e is the elementary charge), that for τ_{pulse} = 10 ns gives j_{th} = 11 A/cm^2. This threshold is low enough to obtain SE under cw excitation: Fig 1. shows the corresponding spectrum, measured with cw pumping at 0.9 μm wavelength.

Obviously, the threshold grows with the SE wavelength and the maximum "operating" temperature T_{max} gets lower. To understand the energetic scale that determines T_{max} let us consider the energy spectrum of Structure #1, presented in Fig.2. One can see that the hole effective mass increases dramatically with k and the dispersion laws in the valence band and the conduction band are no longer quasi-symmetrical. When holes reach larger-mass region the Auger recombination becomes efficient. We have calculated the threshold energies E_{th} for CCHC Auger process (the energetic threshold for CHHH process is high compared to CCHC process, therefore the latter is less important) given in Fig. 2. For both struc-

tures under study we get $k_B T_{max} \approx E_{th}/2$. In Fig. 2 one can see also that the detrimental impact of side maxima in the valence band can be reduced in QW of pure HgTe with the same bandgap as in Structure #1. As easy to see in this case the threshold energy increases significantly.

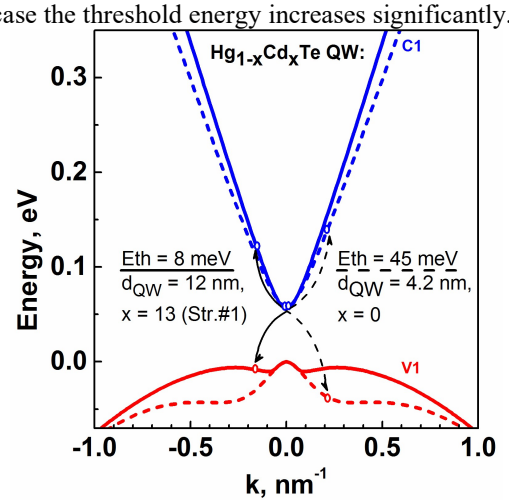

Fig. 2. Calculated energy spectrum of Structure #1 (solid lines) and HgTe/CdHgTe QW with the same bandgap (dash lines), $T = 0$. Threshold energies and carrier configuration are shown for Auger CCHC process.

Effective carrier temperature is affected by their heating by the pumping radiation. At the excitation with radiation wavelength 2.3 μm the carrier heating effect is noticeable already in QW structures emitting at wavelengths μm about 14 μm. For the Structure #1 emitting at λ ~ 20 μm the SE quenching with the increase of pumping power takes place just after the SE arising. We have demonstrated that the pumping with CO_2-laser (λ = 10.6 μm) drastically decrease the carrier heating and the SE intensity monotonously grows with pump power. Thus, the effect of SE quenching with the pump power, observed in Ref.8 is not fundamental but results from using the short wavelength excitation.

Carrier lifetimes are expected to decrease for QW structures with narrower bandgap. The sub-nanosecond carrier lifetimes have been explored via the pump-probe measurements of a sample's transmission using THz free electron laser FELBE at Helmholtz-Zentrum Dresden-Rossendorf[9]. For HgCdTe QW with $E_g = 20$ meV ($f \sim 4.8$ THz) the carrier lifetime proved to be about 100 ps for carrier density 10^{11} cm^{-2} that is sufficient to achieve the population inversion. One can estimate a threshold pumping intensity of 10 kW/cm^2 for an optically pumped laser exploiting such QWs as an active media. Thus, HgCdTe QWs should be able to provide amplification of radiation at interband transitions down to 5 THz (λ = 60 μm).

In conclusion, we demonstrated stimulated emission at wavelengths up to 20.3 μm (14.7 THz) from HgCdTe based waveguide quantum well heterostructures. Nonradiative Auger recombination is shown to be suppressed compared to bulk HgCdTe solid solutions due to the "symmetry" of electron and hole energy-momentum laws. Results of time-resolved pave the way to obtain stimulated emission in wide THz range down to 5 THz.

This work was financially supported by the Russian Foundation for Basic Research (Grants #16-32-60172, #18-52- 16013) and Ministry of Education and Science of the Russian Federation (Grant MK-4399.2018.2). The work was done using equipment of Common Research Center "Physics and technology of micro- and nanostructures" at IPM RAS.

References

1. *Vitiello, M. S., Scalari, G., Williams, B., De Natale, P.* Quantum cascade lasers: 20 years of challenges // Opt. Express. 2015. V.23, No. 4. P. 5167-5182.

2. *Maremyanin, K. V., Ikonnikov, A. V., Bovkun, L. S., Rumyantsev, V. V., Chizhevskii, E. G., Zasavitskii, I.,I., Gavrilenko, V. I.* Terahertz injection lasers based on the PbSnSe solid solution with emission wavelength up to 50 μm and their use for magnetospectroscopy of semiconductors // Semiconductors. 2018. V. 52, No 11 (in press).

3. *Abakumov, V. N., Perel, V. I., Yassievich, I. N.* Nonradiative Recombination in Semiconductors. North-Holland: Elsevier Science Publishers. 1991.

4. *Morozov, S. V., Rumyantsev, V. V., Antonov, A. V., Kadykov, A. M., Maremyanin, K. V., Kudryavtsev, K. E., Mikhailov, N. N., Dvoretskii, S. A., Gavrilenko, V. I.* Time resolved photoluminescence spectroscopy of narrow gap $Hg_{1-x}Cd_xTe/Cd_yHg_{1-y}Te$ quantum well heterostructures // Appl. Phys. Lett. 2014. V. 105, No 2. P. 022102.

5. *Arias, J. M., Zandian, M., Zucca, R., Singh, J.* HgCdTe infrared diode lasers grown by MBE // Semicond. Sci. Technol. 1993. V. 8, No 1S. P. S255-S260.

6. *Dvoretsky, S., Mikhailov, N., Sidorov, Yu. Shvets, V., Danilov, S., Wittman, B., Ganichev, S.* Growth of HgTe Quantum Wells for IR to THz Detectors // J. Electronic Mater. 2010. V. 39, No. 7. P. 918-923.

7. *Morozov, S. V., Joludev, M. S., Antonov, A. V., Rumyantsev V. V., Gavrilenko, V. I., Aleshkin, V. Ya., Dubinov, A. A., Mikhailov, N. N., Dvoretskiy, S. A., Drachenko, O., Winnerl, S., Schneider, H., Helm, M.* Study of lifetimes and photoconductivity relaxation in heterostructures with $Hg_xCd_{1-x}Te/Cd_yHg_{1-y}Te$ quantum wells // Semiconductors. 2012. V. 46, No 11. P. 1362-1366.

8. *Morozov, S. V., Rumyantsev, V. V., Fadeev, M. A., Zholudev, M. S., Kudryavtsev, K. E., Antonov, A. V., Kadykov, A. M., Dubinov, A. A., Mikhailov, N. N., Dvoretsky, S. A., Gavrilenko, V. I.* Stimulated emission from HgCdTe quantum well heterostructures at wavelengths up to 19.5 μm // Appl. Phys. Lett. 2017. V. 111, No 19. P. 192101.

9. *Ruffenach, S., Kadykov, A., Rumyantsev, V. V., Torres, J., Coquillat, D., But, D., Krishtopenko, S.S., Consejo, C., Knap, W., Winnerl, S., Helm, M., Fadeev, M. A., Mikhailov, N. N., Dvoretskii, S. A., Gavrilenko, V. I., Morozov, S. V., Teppe, F.* HgCdTe-based heterostructures for terahertz photonics // APL Materials. 2017. V. 5, No. 3. P. 035503.

Electronic Tunneling and Electric Domains in GaAs/AlAs Superlattices at Room Temperature

I. V. Altukhov[1], M. S. Kagan[1], S. K. Paprotskiy[1], N. A. Khvalkovskiy[1], I. S. Vasil'evskii[2], A. N. Vinichenko[2]

[1]V.A. Kotel'nikov Institute of Radio Engineering and Electronics, Russian Ac. Sci., Moscow, Russia, kagan@cplire.ru
[2]National Research Nuclear University MEPhI, Moscow, Russia

One of the main problems in the development of semiconductor sources of the THz radiation is their operation at room temperature. Operation frequencies of room-temperature hot-electron bulk semiconductors such as Gunn diodes are limited by the time of development of the negative differential conductivity and the dielectric relaxation time. The former time in most semiconductors is usually in the range of picoseconds. The Maxwell relaxation time at the conventional doping level on the order of 10^{15}cm^{-3} is also ~10^{-12} s. Therefore, the operation frequency band of hot-electron devices does not exceed 100–200 GHz. This limit is eliminated by using the laser scheme, when the energy of a photon is determined by the difference between energy levels with the inverse population and does not depend on the inertia of the conductivity relaxation. However, all THz semiconductor lasers operate at cryogenic temperatures. It is hardly possible to implement the population inversion at room temperature, since kT = 25 meV and the energy of THz photons is ~10 meV. Therefore, it is reasonable to search for systems with a negative high-frequency differential conductivity, which can excite oscillations in the corresponding cavity. Good examples are resonant-tunneling diodes, in which the generation frequency has been reached 1.92 THz [1]. Another suitable semiconductor systems are superlattices (SLs).

The electron transport in semiconductor SLs has been studied in detail in recent decades [2], mainly in connection with the predicted amplification of Bloch waves, which can make it possible to create tunable sources of THz radiation. The main hindrance to the Bloch wave amplification is the formation of electrical domains owing to the static negative differential conductivity (NDC) arising in superlattices at resonant tunneling between confined states in neighboring quantum wells [3]. The domain formation in superlattices eliminates the Bloch gain. On the other hand, the samples with the electrical domains can exhibit the dynamic NDC (the real part of electrical impedance is negative) in some frequency range (similarly to bulk materials [4-8]) and can be used for high-frequency generation in a suitable resonant cavity.

Superlattices for the THz range should satisfy several conditions. To get the short conductivity relaxation time, which is the time of tunneling in SLs, one has to use SLs with thin barriers. To prevent a thermal exchange with carriers between succeeding confined states in SLs, we need to have narrow quantum wells and the large band offset. For fast space charge redistribution in SLs with electric domains, the high doping level is needed to obtain the short dielectric relaxation time. Here we present studies of tunneling electronic transport in short-period GaAs/AlAs superlattices (SLs) with electric domains.

The MBE grown GaAs/AlAs SLs consisted of 100 periods of 4 nm GaAs/2 nm AlAs between heavily doped (~10^{19}cm^{-3}) n^+ cap layer and n^+ substrate. GaAs quantum wells (QWs) were Si doped with concentration of $2*10^{17}$cm^{-3}. The ring-shaped mesa structures with the diameters from 10 to 15 μm and 0.8 to 1.5 μm widths (Fig. 1) formed the distributed THz cavity with resonant frequencies corresponding to the free-space wavelengths from ~110 to ~170 μm. Triangular voltage pulses with a sweep-up times of 0.5 to 10 μs and sweep-down times up to 100 μs applied to the sample were used to record I-V curves. Measurements were performed at room temperature.

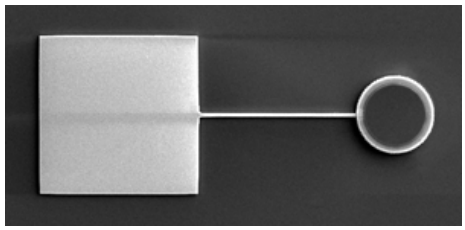

Fig. 1. View of the sample with the contact and current lead

The moving domains are formed at some threshold voltage and became apparent in a sharp decrease of current (up to 50% - Fig. 2). It was found that this threshold voltage changes considerably under the change of the cavity [9]. The cavity was changed by deposition of a droplet of conductive silver epoxy paste covering the entire top part of the mesa structure (see insets in Fig. 2). Fig. 2 shows the current–voltage

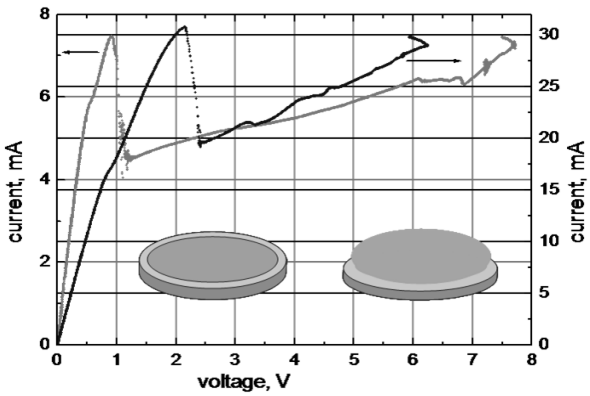

Fig. 2. Current–voltage characteristics of the GaAs/AlAs SLs under a change of the cavity: (lower curve) before and (upper curve) after the deposition of a droplet.

characteristics of the structure before and after the deposition of this droplet. The current through the sample after the deposition increased, what is natural because the contact area increased. In fact, the increase in the current approximately corresponds to the increase in the area. In addition, the threshold field of the domain formation changed, which was generally surprising because the thickness of the structure (the distance between current contacts) remained the same.

The possible origin of the change in the threshold field at changing the contact area is the appearance of an alternating field with sufficiently high amplitude in the cavity. Indeed, if an ac voltage of comparable amplitude is applied to the sample with a nonlinear current–voltage characteristic in addition to the dc voltage, an additional dc voltage appears because of the detection and shifts the operating point. Thus, this experiment indicates the excitation of THz oscillations in the cavity owing to the negative resistance of the superlattice with domains. We note that an analogous effect of an alternating electric field on the shape of direct current–voltage characteristics was observed in the bulk GaAs with the Gunn effect [10].

For not resonated structures, several features appeared in I-V curves (Fig. 3). First one is the hysteresis at forward and backward bias sweep. The size and shape of hysteresis loop depends on the peak voltage of the triangular pulse. The maximal loop observed when the current grows up to its peak value in the I-V curve. In this case the current saturation appears in some voltage range (Fig. 3), being essentially larger at bias sweep-down. The current saturation is due to static domain formation. So, the current hysteresis can be explained by a transition from moving to static field domain at sweeping the bias up and the return at its sweeping down. The large asymmetry of the transition times was found: the transition from travelling to static domain regime passes in a time shorter 0.1 microsecond, while the time of the reverse transition - from static to travelling domain regime – is ~100 microseconds. It is seen from I-V curves in Fig. 3 measured at different sweep-down duration. The long time is referred to deep impurities at the SL-buffer layer boundary.

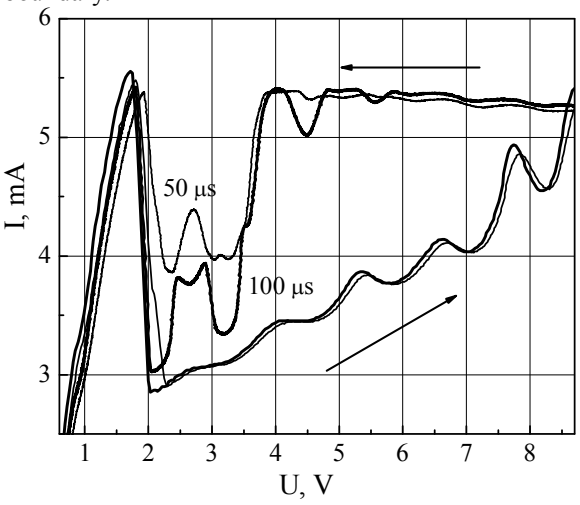

Fig. 3. I-V curves at different voltage sweep-down times

The second feature is the series of almost voltage-periodic maxima in current-voltage characteristics. The maxima are on a background of current rise in the mean. The current rise is evidence of triangular form of the domain: the negative charge at one of domain boundaries (in one quantum well) is due to free electrons with the concentration of more than one order larger than the donor concentration supporting the necessary field step, while the positive charge at opposite domain boundary is due to positively charged donors [11, 12]. The linear spatial grows of electric field inside the domain is just the result of donor depletion.

The positions of the maxima in the I-V curves did not depend on the frequency of THz cavity, they coincided at different ring cavity diameters, while essentially changed at cooling. The average period of the maxima at nitrogen temperature was by 1.5 times larger than that at room temperature. The origin of these maxima is attributed to the optical phonon assisted tunneling between quantum wells inside the triangular domain.

The work was supported by RFBR grant 16-29-03135

References

1. *Maekawa, T., Kanaya, H., Suzuki, S., Asada, M.* Oscillation up to 1.92 THz in resonant tunneling diode by reduced conduction loss // Applied Physics Express 2016. V. 9, No. 2. P. 024101

2. *Wacker, A.* Semiconductor superlattices: a model system for nonlinear transport // Physics Reports, 2002. V. 357, P. 1

3. *Klappenberger, F., Alekseev, K. N., Renk, K. F.*, et al. Ultrafast creation and annihilation of space-charge domains in a semiconductor superlattice observed by use of Terahertz fields // Eur. Phys. J. B 2004. V. 39, P. 483

4. *Thim, H. W.*, Linear microwave amplification with Gunn oscillators // IEEE Trans. Electron. Dev. 1967. V. 14, P. 517

5. *Hakki, B. W.* Amplification in Two-Valley Semiconductors // J. Appl. Phys. 1967. V. 38, P. 808

6. *Zhdanova, N. G., Kagan, M. S., Kalashnikov, S. G.* Impedance of semiconductor with static domain // Sov. Phys. Semicond. 1974. V. 8, P. 1121; 1126

7. *Altukhov, I. V., Kagan, M. S., Kalashnikov, S. G., et al.* Electromagnetic wave amplification by Gunn diodes with moving domains // Sov. Tech. Phys. Lett. 1980. V. 6, P. 237

8. *Kagan, M.S., Landsberg, E.G., Chernyshov, I.V.* Negative conductivity due to vibrations of the wall of a static domain, Sov. Phys. Semicond. 1984. V. 18, P. 615

9. *Altukhov, I. V. Dizhur, S. E. Kagan, M. S.*, et al. Effect of a Terahertz Cavity on the Conductivity of Short-Period GaAs/AlAs Superlattices // JETP Letters 2016. V. 103, No. 2, P. 122

10. *Altukhov, I. V. Kagan, M. S. Kalashnikov, S. G., et al.* Electrical instability of a semicondutor with a negative differential conductivity due to simultaneous heating of electrons by static and alternating electric fields // Sov. Phys. Semicond. 1978. V. 12, P. 172

11. *Suris R. A.* Inhomogeneous structures in semiconductors with superlattices // Sov. Phys. Semicond. 1973. V. 7, No. 8 P. 1035

12. *Bonilla, L. L., Grahn H. T.* Non-linear dynamics of semiconductor superlattices // Rep. Prog. Phys. 2005. V. 68, No. 3, P. 577

Wideband Josephson THz flux-flow oscillator integrated with the slot lens antenna and the harmonic mixer

N.V.Kinev[1], K.I. Rudakov[1,2,3], L.V. Filippenko[1], A.M. Baryshev[3], V.P. Koshelets[1]

[1]Kotel'nikov Institute of Radio Engineering and Electronics of RAS, 125009 Moscow, Russia, nickolay@hitech.cplire.ru
[2]Moscow Institute of Physics and Technology, 141701 Dolgoprudny, Russia
[3]University of Groningen, 9712 CP Groningen, Netherlands

Introduction

Terahertz (THz) wideband sources are required nowdays in many field, such as spectroscopy, astronomy and radio physics. We present a new implementation for a flux-flow oscillator (FFO) based on a long Josephson junction providing the THz emission in the open space. The FFO was used earlier in our team merely as an on-chip heterodyne for the SIS receiver [1-2], it has a really wide operating range up to 100% of central frequency and a power of about 1 μW. Based on the Nb/AlN/NbN trilayer the FFO with dimensions 400x16 μm^2 provides the output radiation from 200 GHz up to 750 GHz with the spectral linewidth of about 1 MHz. The upper operating frequency can reach 1 THz. The phase-lock loop (PLL) is used for the phase locking of the emission collecting up to 97% of the output THz power in the peak with a width of about 40 kHz. Such oscillator implemented as an external source could be useful for many tasks – gas spectroscopy, heterodyne receivers, etc.

Concept of the THz oscillator & numerical simulations

The principle of the FFO operation is discussed elsewhere [3-4]. The operating frequency is defined strictly by the Josephson equation

$$hf = 2eV, \qquad (1)$$

where V is the DC voltage on the junction. The original idea of this work is the integration of the FFO with a harmonic mixer (HM) for the feedback locking loop and a transmitting slot antenna on a single chip (fig. 1a) placed on the back surface of the elliptical lens (fig.1b). The chip substrate and the lens are both made of silicon. Thus, the main task is the coupling of the oscillator having low output impedance (less than 1 Ω) to the lens antenna having high impedance (tens of Ω) and forming a beam pattern required for applications, and simultaneous coupling to the harmonic mixer based on SIS junction having the area about 1 μm^2 and the impedance of about several Ω. Coupling to the antenna should be as high as possible, while coupling to the HM should be just enough for properly PLL operation and not take away much power (commonly 10-20 %). Both couplings with the antenna and the HM should be in the same frequency range, which is required to be as wide as possible. The slot antenna is fabricated of superconducting Nb thin film, as well as the transmitting microstrip lines between the FFO, antenna and HM (the thickness is about 200-450 nm). The chip with the planar integrated circuit mounted on the lens is placed in the liquid helium cryogenic system with the temperature 4.2 K.

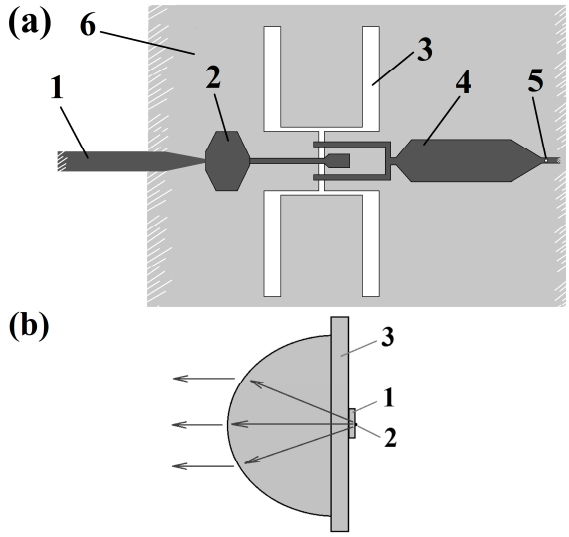

Fig. 1. (a) layout of the planar structure of THz oscillator (1) based on a long SIS junction coupled by microstrip line (2) to slot antenna (3) and by microstrip line (4) to harmonic SIS mixer (5), metallization layer (6) of antenna is also the bottom electrode of the microstrip and the SIS junctions; **(b)** scheme of the chip (1) with oscillator and antenna shown on (a) placed at the far focus (2) of the silicon lens (3). The scheme (b) is not to scale.

The main calculations for the designs of the oscillator coupled to the antenna and HM are made by using the specialized software for microwave 3D modeling. Three designs of the "oscillator & antenna structure" were developed for the central frequencies 350 GHz, 450 GHz and 600 GHz, hereinafter called A-350, A-450 and A-600 respectively. More than 70% of oscillator output power is radiated in the ranges of 250 – 410 GHz, 330 – 570 GHz and 420 – 700 GHz for three designs, the calculation results for the emitted power vs frequency will be shown together with the experimental results in the next section. Designs A-450 and A-600 contains all the elements shown in fig.1a, but A-350 doesn't contain the HM with a corresponding coupling line and has no ability to lock the oscillator. A-350 design will be upgraded in the next step of this work. In the fig. 2 the calculated beam patterns at the fixed frequency for 350 GHz, 450 GHz and 600 GHz antenna designs are shown, the main power is concentrated in the center lobe.

Experimental results: preliminary testing

The batch of experimental samples based on Nb/AlN/NbN was fabricated according to the developed designs. The current density of the SIS trilayes on the batch is about j_c = 10kA/cm^2, this corresponds to parameter R_nS of about 20 Ω·μm^2. The quality fac-

tor of the junctions defined as the ratio of "sub-gap" resistance to normal resistance R_j/R_n is about 30.

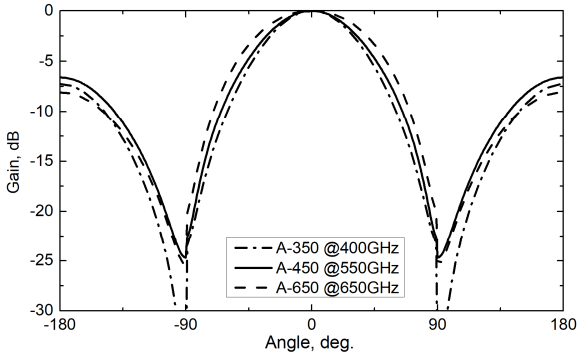

Fig. 2. Numerically simulated beam patterns of three antenna designs at the fixed frequency in the region of operation.

The pumping of the SIS harmonic mixer by FFO power leads to the appearance of current quasiparticle step on the IVC which is measured directly in the whole frequency range of the FFO operation. In the fig.3 the experimental results for frequency dependences of HM pumping are presented together with the calculation results of the absorbed power for the designs A-450 and A-600. There is a good agreement of the experiment with numerical simulations.

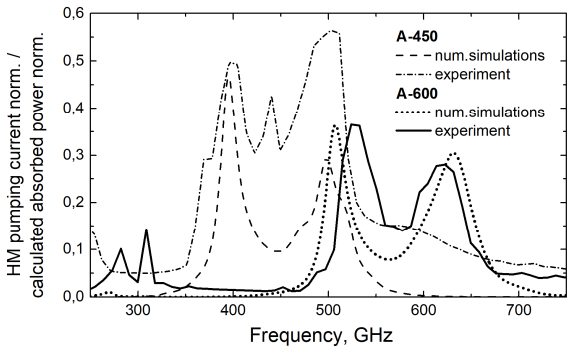

Fig. 3. Experimental results of HM pumping by FFO power and calculation results of the absorbed FFO power by HM. The HM pumping current is normalized to the "current jump" at the gap SIS voltage. The absorbed power is normalized to the total output FFO power.

For the measurements of the FFO emission in the open space by lens antenna the superconducting integrated spectrometer (SISP) is used [5]. Two liquid helium cryostats for the oscillator and the receiver were used and set opposite each other, so that the quasioptical windows of the cryostats were oriented toward one another. The local oscillator of 19-21 GHz is used for the mixing by the HM of the FFO signal and the *n*-th harmonics of the oscillator. Additionally, the PLL system is used for locking the signal. The radiated spectral line could be measured simultaneously by the HM in the intermediate frequency (IF) range 0 - 800 MHz and by the spectrometer in the IF range 4 - 8 GHz. The emission in the open space was successfully obtained in the wide region at some frequency points of operation and studied by the SISP as well as by the HM and the feedback loop. The results of the first measurements together with the transmitting antenna characteristics are shown in the fig.4. The spectral lines emitted by FFO have the Lorenzian shape with a linewidth of about 2-15 MHz; the ratio of signal (spectral line) power to noise power is shown on the right axis in fig.4. Numerical simulations for A-350 (250 - 410 GHz range) are not presented since an experiment still was not carried out at THz frequencies for this design. Such experiment requires another type of receiver (a Golay cell or a Si bolometer).

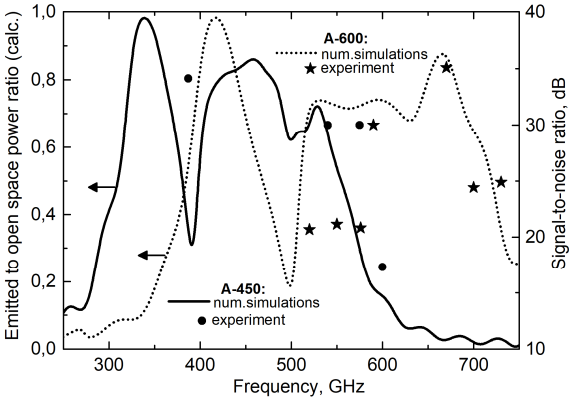

Fig. 4. Calculation results of power emitted by antenna to open space normalized to the total output FFO power (left axis); experimental points of output emission detected by SISP at some frequencies (right axis).

Conclusion

The superconducting THz oscillator based on the long Josephson junction with unidirectional flow of the fluxons (a flux-flow oscillator or a FFO) is an encouraging solution of the THz source for the tasks where wideband frequency tuning is required and the high power is not necessary. We proposed the idea and implementation for the external THz source based on the FFO integrated with the harmonic mixer and the transmitting slot antenna integrated on a single chip with the oscillator. The lens is used forming the narrow beam pattern. Three antenna designs that covers the 0.25 - 0.7 THz region are developed and numerically simulated, two designs for 0.33 - 0.57 THz and 0.42 – 0.7 THz are experimentally studied. The emission to open space is measured by external high resolution spectrometer.

This work is supported by Russian Science Foundation (project № 17-79-20343).

References

1. *Koshelets, V.P., Shitov, S.V.* Integrated Superconducting Receivers // Supercond. Sci. Technol. 2000. V. 13. P. R53-R69.

2. *Lange, G., Boersma, D., Dercksen, J. et al*. Development and Characterization of the Superconducting Integrated Receiver Channel of the TELIS Atmospheric Sounder // Supercond. Sci. Technol. 2010. V. 23. 045016 (8pp).

3. *Nagatsuma, T., Enpuku, K., Irie, F., Yoshida, K.* Flux-flow type Josephson oscillator for millimeter and submillimeter wave region // J. Appl. Phys. 1983. V. 54 P. 3302-3309.

4. *Zhang, Y.* Theoretical and experimental studies of the flux-flow type Josephson oscillator. 1991. Gothenburg: Chalmers University of Technology.

5. *Koshelets, V.P., Dmitriev, P.N. et al.* Superconducting Integrated Terahertz Spectrometers. // IEEE Trans. Terahertz Sci. Technol. 2015. Vol. 5, No. 4. P. 687-694.

Evidence of synchronization of large Josephson-junction arrays by traveling electromagnetic waves

M.A. Galin[1,2], E. A. Borodianskyi[2], V. V. Kurin[1], I. A. Shereshevskiy[1], N. K. Vdovicheva[1], V. M. Krasnov[2], and A.M. Klushin[1]

[1]Institute for Physics of Microstructures RAS, Nizhny Novgorod, Russia, a_klushin@ipmras.ru
[2]Department of Physics, Stockholm University, AlbaNova University Center, Stockholm, Sweden

The Josephson effect can be used for the generation of high-frequency electromagnetic radiation [1]. The frequency is limited only by the superconducting energy gap. For achieving a practically important mW level of emission power the arrays containing $N \sim 10^4$–10^5 JJs would be needed. Such arrays would have a typical size of $L \sim 1$ cm, which is much larger than the wavelength λ even at sub-THz frequencies. The substantial phase delays between JJs are the significant problem impeding the synchronization of large JJ arrays.

It was recently suggested [2, 3] that the synchronization of large JJ arrays can be mediated by a unidirectional traveling wave along the array. The main fingerprint of the traveling-wave regime in an oscillating system is a strong forward-backward asymmetry of the radiation pattern. This is qualitatively different from the resonant, standing-wave case, which per definition has a symmetric radiation pattern. Thus, the shape of the radiation pattern allows a clear distinction of the two scenarios.

In our work we have studied angular dependence of electromagnetic wave emission from two large Nb/NbSi/Nb JJ series arrays having different design. For both arrays we observe a significant forward-backward asymmetry of the measured radiation patterns which is interpreted by the involvement of the traveling-wave mechanism of synchronization. We have also performed numerical simulations of the Josephson traveling-wave antenna which have supported our conclusions.

The studied arrays contain 6972 and 9000 JJs which are located on silicon substrates, on the area of 5×5 mm. The first sample was named as linear array while the second was named as meander array. More details about characterization of the arrays can be found in Ref. [4]. Electromagnetic radiation was detected by a high-purity *n*-doped InSb bolometer which was preliminarily calibrated. Measurements are performed in a closed-cycle cryostat with a sample-in-gas cooling and the base temperature $T = 1.8$ K. Array can be rotated by special gear mechanism while the detector is permanently fixed. The detector is located at approximately 1 cm from the geometrical center of the array. Position of the detector face-to-face on top of the array corresponds to the angle $\alpha = 90°$. The relative accuracy of the rotator is 0.02°.

We performed measurements of current-voltage characteristics (IVCs) at different α simultaneously with measurements of the detected power. It was obtained that critical current of both JJ arrays is $I_c \sim 3$ mA and the steps in the IVCs appear in the range $U \sim 2$–2.5 V.

The angular measurements were performed in the stable steps of IVCs. An analysis of the angular dependencies of the emission power reveals a forward-backward asymmetry of the radiation patterns for both samples. In the Fig.1 the radiation pattern measured for the meander array was shown. It represents decreases of zero-bias resistance $-\Delta R_{det}$ relative to the case of unbiased array. Measurement was made at $U = 2.223$ V corresponding to oscillation frequency $f = 119.3$ GHz. As seen, the radiation pattern demonstrates a pronounced asymmetry in emission between forward ($\alpha < 90°$) and backward ($\alpha > 90°$) directions. Similar, but less prominent, asymmetry of radiation power is demonstrated by the linear array. Such asymmetry is inconsistent with the resonant mechanism of synchronization of the arrays by standing waves because standing waves per definition should have forward-backward symmetric radiation patterns.

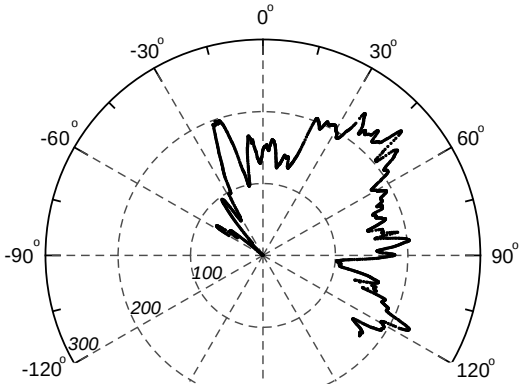

Fig. 1. Measured angular dependence of the ac-detected signal $-\Delta R_{det}$ (Ω) for meander array

The emission power reached the maximum values $P_{em} \sim 80 - 90$ μW for both arrays. For the linear array it occurs at the step in the resistive branch of IVC. However for the meander array it occurs outside the step in the reverse branch of IVC near $U = 1.8$ V (see Fig.2, inset). This suggests that traveling waves play a more prominent role in the emitted electromagnetic field for the meander, than for the linear array.

In Fig.2 the dependence of detected emission power of meander array along the reverse branch of the IVC is demonstrated. Here the dc-voltage response was registered $-\Delta U_{det}$ and the data was obtained at $\alpha = 40°$ when the maximal power was attained (Fig.2, inset). During the sweeping from a large bias current downward to zero the junctions switch in sequence from the resistive into the zero-voltage state. Thus, variation of the emitted power with bias voltage

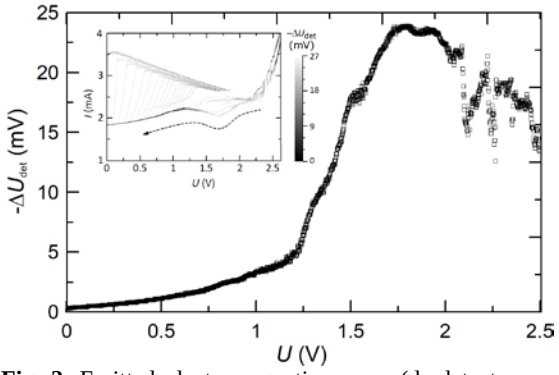

Fig. 2. Emitted electromagnetic power (dc-detector response, $-\Delta U_{det}$) along the reverse branch of the IVCs of meander arrays at α = 40°. In the inset the corresponding IVCs obtained by repeated back-and-forth sweeping of bias current is shown. The gray bar indicates the detected power (dc-detector response)

is primarily due to variation of the number of oscillating junctions N_a, approximately proportional to voltage U. It is seen that a rapid superlinear enhancement of the emission power occurs at 1.3 V. It is known that for the case, when all the oscillating junctions are in the exactly identical state, the emission power should increase as $P_{em} \sim N^2$. Thus the data in Fig.2 indicate the regime of superradiant emission in the meander array. It is suggested that a nonresonant traveling-wave mechanism of synchronization contributes to the observed superradiant emission in the meander array, along with persisting standing-wave resonances that is indicated by the presence of steps in the IVCs.

As suggested earlier [2, 3] large JJ arrays may act as Josephson traveling-wave antennas. Such antennas have asymmetric radiation patterns with a maximum in the direction of propagation of the wave at an angle $\alpha = \arccos h/k$, where h is the wave number of current oscillations in the antenna and k is the wave number of the emitted wave in vacuum. For analysis of nonlinear dynamics of the Josephson traveling-wave antennas, we develop a numerical code for solving Maxwell equations by the FDTD method in combination with self-consistent solution of junction dynamics within the RSJ model.

Our simulated array contains 10 JJs, linear lumped passive elements and two voltage sources (Fig.3a). Elements in the arrays are connected by perfectly conducting wires. The array is placed on dielectric substrate a dielectric permittivity 10. Junction parameters used in simulations are I_c = 2.5 mA, normal resistance 0.5 Ω, and the McCamber parameter 0.2. We inserted passive elements (resistances and inductances with the values of 25 Ω and 200 pH, respectively) which are different at the opposite sides of the circuits. These elements are needed for simulating the dynamical violation of the symmetrical state that has to take place in real JJ arrays.

Numerically simulated radiation pattern are shown in Fig. 3b. The chosen radiation frequency f = 136.6 GHz provides the wavelength of the current wave considerably smaller than the dimension of the circuits

It is seen that array exhibit a pronounced forward-backward asymmetry of radiation patterns with max-

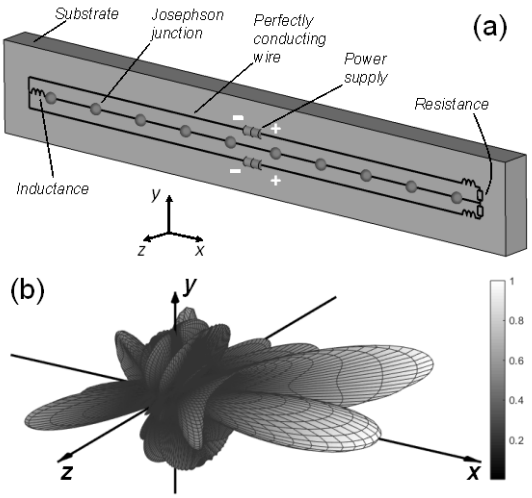

Fig. 3. The model of Josephson traveling-wave antenna (a) and simulated three-dimensional radiation pattern (b)

imum in the direction of positive x-axis direction. The value of directivity in the maximum power radiation is 4.6 dBi. The radiation pattern has two large lobes with equal amplitudes. One of them is directed strictly along the x-axis that indicates a surface plasmon excited in the array. The relation $h/k > 1$ is realized in this case. For another large lobe $h/k < 1$, i.e. an ordinary traveling wave exists with the finite angular deviation α from the x-axis which is α = 42° in this case.

The aim of these simulations was rather to demonstrate that the main evidence for the traveling-wave regime is the forward-backward asymmetry of the radiation pattern with a maximum in the traveling-wave direction. This is qualitatively consistent with the observed forward-backward asymmetry of emission from the studied large JJ arrays.

The work was supported by the Russian Foundation for Basic Research (Grants No. 16-32-00686 and No. 18-02-00912), the Swedish Foundation for International Cooperation in Research and Higher Education (Grant No. IG2013-5453), and the Swedish Research Council (Grant No. 621-2014-4314). V. V. K. and A. M. K. would also like to acknowledge the partial support of this research by the Russian Science Foundation (Grant No. 15-12-10020).

References

1. *Yanson, I. K., Svistunov, V. M., Dmitrenko, I. M.* Experimental observation of the tunnel effect for cooper pairs with the emission of photons // Zh. Eksp. Teor. Fiz. 1965. V. 48, P. 976 [Sov. Phys. JETP 1965. V. 21, P. 650–652].

2. *Galin, M. A., Klushin, A. M., Kurin, V. V., Seliverstov, S. V., Finkel, M. I., Goltsman, G. N., Müeller, F., Scheller, T., Semenov, A. D.* Towards local oscillators based on arrays of niobium Josephson junctions // Supercond. Sci. Technol. V. 28, P. 055002.

3. *Kurin, V. V., Vdovicheva, N. K., Shereshevsky, I. A.* Josephson traveling-wave antennas // Radiophys. Quantum Electron. 2017. V. 59, P. 922–936.

4. *Galin, M. A., Borodianskyi, E. A., Kurin, V. V., Shereshevskiy, I. A., Vdovicheva, N. K., Krasnov, V. M., Klushin, A. M.,* Synchronization of large Josephson-junction arrays by traveling electromagnetic waves // Phys. Rev. Applied. 2018. V. 9, P. 054032.

Long-Pulsed Modulation Regimes of Subterahertz Nanosecond Waveguide Switches

Maxim L. Kulygin[1], G. G. Denisov[1,2], A. P. Fokin[1], E. A. Novikov[1], S. H. Salahetdinov[1], S. V. Shubin[1], I. A. Litovsky[2]

[1]Institute of Applied Physics RAS, Nizhny Novgorod, Russia, kmaxim@appl.sci-nnov.ru
[2]Lobachevski State University, Nizhny Novgorod, Russia

INTRODUCTION

Sub-terahertz resonator cavity-based switches [1, 2] with an active semiconductor element of Gallium Arsenide (GaAs) driven by laser pulses are used to cut microwave signal from a generator to series of wave packets. Intrinsic properties of Gallium Arsenide crystal help to achieve nanosecond level of switching performance with green driving laser emission [3]. The resonant waveguide cavity construction ensures low phase distortion to the packets' at the output [4]. The output phases are linked to each other once the input microwave signal is coherent, e.g. a gyrotron in a phase stabilization regime [4, 5]. The prospective application of the switches is the new generation of DNP-NMR (Dynamic Nuclear Polarization – Nuclear Magnetic Resonance) spectroscopy featuring low power on probing objects and expanded resolution.

OVERVIEW OF THE SWITCH

A photo of the 260 GHz waveguide semiconductor switch used for the second-long pulse modes is shown at Fig. 1. Microwave input and output are symmetrical IEA WR3 standard rectangular waveguides – 0.864 x 0.432 mm – to the left and right flanges shaped according to UG 387 international standard. There is a rectangular input hole with the dimensions of about 0.55 mm in the center for driving laser pulses. A semiconductor plate of gallium arsenide is installed right under the laser input hole. The switch can be slightly fine-tuned by about a 10 GHz with a mechanical tuning screw (not shown on the picture).

MICROWAVE POWER MEASUREMENT PROBLEM

Testing the switch for the first time demonstrated safe operation with no heating issues with about 30 mW test power source at the input. The maximum possible microwave power the switch can commutate is limited by an IEA WR3 waveguide standard safety value for 260 GHz frequency band; it is about 20 W, about two times lower than the breakdown value. A trivial way to raise the power up to the maximum of 20 W is a challenge because of very limited measurement precision. Modern gyrotrons are usually designed to provide power up to kilo- and megawatts, and commonly used power meters (or wattmeters) are calorimeters rated to the corresponding maximum power levels. They produce errors of worse than 100% for 20 W and lower powers. The lower powers are possible to register with semiconductor detectors.

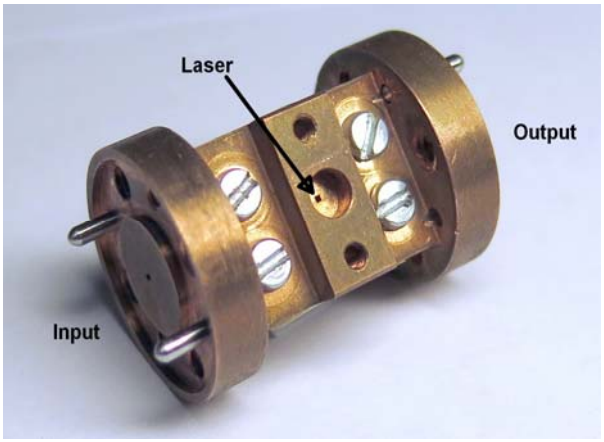

Fig. 1. Photo of the 260 GHz resonant cavity-based switch.

But there are still problems of matching the detectors preventing spurious reflection. Up to now there are no high-precision commercial wattmeters for low powers for frequency band of 260 GHz [6].

CHANGING THE PROBLEM TO LASER MEASUREMENTS

Meanwhile, the most of lasers are known for more than 50 years, and their power is easy to measure with high precision in wide ranges of powers for common wavelengths. So substituting the Ohmic heating mechanism by commutated microwaves with an appropriate laser absorption in the semiconductor, we can recalculate the laser power value to the corresponding microwave one. The semiconductor plate heated by an infrared laser demonstrates the same temperature distribution as it is heated by a commutated microwaves. Both the functions decay smoothly into the depth, and the maximum values for the functions are achieved at the plate's surface. For a 1.06 μm laser it is known that about R = 1/3 of the power is reflected from gallium arsenide, and the rest is absorbed in the semiconductor. The microwave power insertion loss coefficient for 260 GHz switches is about -0.5 dB, i.e. about T = 10%. Let us consider the switch is able to endure the maximum laser power of P_L. So, for the maximum endurable microwave power we can write:

$$P_M = \frac{(1-R)}{T} \cdot P_L \sim 7 \cdot P_L \qquad (1)$$

The experiments have shown that the 260 GHz waveguide semiconductor switches designed for nanoseconds are able to make pulses up to a second. Therefore the switches cover at least nine orders by duration,

from 1 nanosecond to 1 second and even longer. The switching capabilities at longer durations depend on the pulse length and form, the power and energy of the laser pulse, and the microwave power the switch commutates. There is no case that should be called optimum for switching; it always depends on an application the switch is used within. The maximum commutated microwave power the switch should withstand can be estimated with a substitution of two heating mechanisms in gallium arsenide, the infrared laser one and the microwave Joule one. The switch has successfully passed a 1-second 1-Watt laser pulse, and 1 second is much more than all the relaxation times in the switch. So we can estimate the switch should withstand:

$$P_M = 7 \cdot P_L = 7W \qquad (2)$$

The maximum safety transmittable power through an IEA standard WR3 waveguide, 0.864 x 0.432 mm, is about 20 W. While we have seen the semiconductor plate has damaged after the 20 W laser experiment, we have managed to capture the moment of blow and conclude the minimum operable pulse duration is 15 ms under that maximum laser power.

The switch has been repaired after the blow and further experiments have been performed with a 1 kHz pulsed laser. The laser has been shuttered on and off with an optical gate with operating durations from 100 μs to 1 ms to support different heating regimes of the semiconductor plate to make future blowouts virtually impossible.

THE VERY FIRST EXPERIMENT WITH GYROTRON

To confirm these simple theoretical estimations, (1) and (2), we performed a plain test with a gyrotron. The gyrotron [5] provides second-long microwave pulses at the frequency of about 258 GHz with the power rate of about 100 W and Gaussian beam aperture of about 35 mm. The switch has an input rectangular waveguide with dimensions 0.864 x 0.432 mm corresponding to IEA WR3 standard. So to obtain the input power of several Watts we have attached a 7 x 4 mm horn to the input of the switch. Therefore the estimated power in the real experiment is about 3.5 W. The maximum length of the gyrotron's pulse is 8 s; it was limited by the power transmission line and cooling. No laser has been used so the switch is always in the ground state.

Fig.2 displays the main characteristic of the switch in the ground state when the switch is closed and the microwave power does not pass through, the insertion loss before and after the gyrotron's microwave pulse. We can see that after the pulse the main resonance became deeper, about -5.5 dB compared to about -4.7 dB before the test. The resonance always vanishes if the semiconductor plate is burned out. But now we can see quite a contrary case. It can be explained the way the semiconductor plate has not been burnt out under the 3.5 W 8 s gyrotron pulse, it even got better since only the remained dirt (occasional fingertips, organics and dust from the air) has been burnt out.

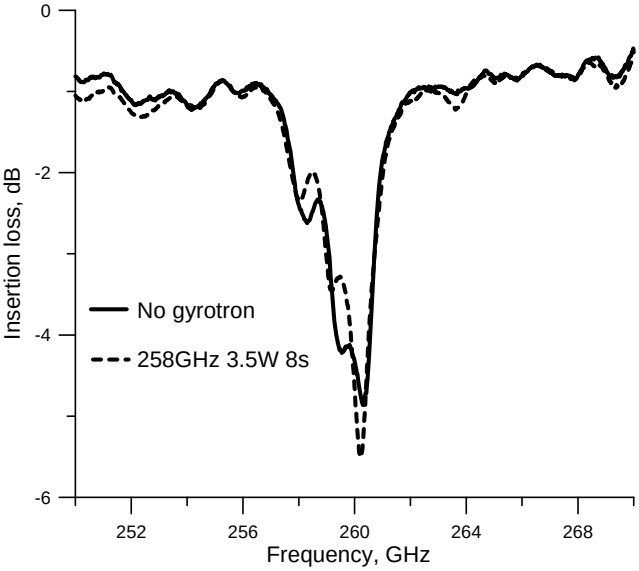

Fig. 2. Insertion loss of the switch in the ground state, solid line is before the gyrotron pulse, dashed line is after the pulse.

The switch has successfully passed the test and we can conclude that the gyrotron's radiation can be useful for final cleaning of the switch.

CONCLUSION

The second-long pulses have been produced with the switches intended for nanosecond-long pulses. So the switches have demonstrated the pulse range of about 10 orders, from 800 ps to 8 s at 260 GHz. Using the switches at the second-long pulse regimes is more important than just a scientific curiosity. It provides the ability to overcome the shortage of low-precision power measurement in sub-terahertz region by changing the problem to well-known low-cost commercial laser measurements that are easily available in every laser-equipped laboratory. We have predicted theoretically our switch is tough to withstand no less than 7 W of microwave commutated power. And we have proven it partially in the experiment with 3.5 W gyrotron. The switch has not been damaged; it's even got better quality. So the gyrotron test should be included in the switch production sequence further to improve quality.

The project is supported by the Russian Foundation for Basic Research, Grant No. 15-08-03158.

References

1. K*ulygin M., Denisov G.* Nanosecond Laser-Driven Semiconductor Switch for 70 GHz Microwave Radiation // J. Infrared mm THz w., V. 33, No. 6, p. 638-648.

2. *Kulygin M. L., et al.* Development of Waveguide Semicond. Switch. of Microw. Rad. in the 70- and 260-GHz Ranges // Radiophys. Quant. El., V. 57, No. 7, p. 509-518.

3. *Kulygin M., Denisov G., Vlasova K., et al*. Nanosecond Microwave Semiconductor Switches for 258…266 GHz // J. Infrared mm THz w., *V.* 36, No. 9, p. 845–855.

4. *Kulygin M. L., Shubin S. V., et al*. 260 GHz Laser-Driven Semiconductor Switches with Performance Rate up to Nanosecond. *Proc. IEEE COMCAS 2015 Int. Conf.*

5. *Glyavin M., et al*, Gyrotron Freq. Stab. by a Weak Ref. W. // *Radiophys. Quant. El*., V. 59, No. 9, p. 673-683.

6. *Kulygin M., et al.* Subterahertz Nanosecond Switches Driven by Second-Long Laser Pulses // *IEEE Trans. THz Sci. Tech.,* V. 7, No. 2, p. 225-227.

Active Josephson traveling wave antennae as prospective terahertz oscillators

V. V. Kurin, N. K. Vdovicheva, I. A. Shereshevskii

Institute for Physics of Microstructures RAS, Nizhny Novgorod, Russia, kurin@ipmras.ru

A terahertz superconducting oscillators based on large amount of Josephson junction embedded in open system guiding traveling electromagnetic wave is theoretically considered and computer simulated. It is shown that such active Josephson antennae represent oscillator effectively radiated into open space with power scaled with the system size and number of junctions. Dynamics and directivity patterns of such Josephson antennae depending on bias current is investigated and it is shown that such oscillator with sufficiently large junction amount can be competitive with quantum cascade lasers.

It is well known that the Josephson Effect can be used for the generation of high-frequency electromagnetic radiation. The frequency is limited only by the superconducting energy gap. For low-Tc superconductors the frequency is in the sub-THz range and for high-Tc superconductors it can be up to approximately 20 THz. But the emission power from a single Josephson junction is quite small. It can be considerably enhanced provided coherent contribution of many, $N \gg 1$, Josephson junctions to radiated electromagnetic field.. For achieving a practically important mW level of emission power very large arrays containing $N \sim 10^4 - 10^5$ Josephson junctions would be needed. Taking into account the attainable integration density, such arrays would have a typical size of $L \sim 1\,\text{cm}$, which is significantly larger than the wavelength λ even at sub-THz frequencies.

The larger the array is the more difficult is the synchronization. This is caused by large phase delays along the array. Recently, it was suggested [1] that the synchronization of extremely large arrays can be mediated by a unidirectional traveling wave along the array, qualitatively similar to the operation of a traveling wave Beverage-type antenna [2].

In this work, we consider such large-size Josephson systems and present their theoretical description and computer simulation. We demonstrate that in some classes of such systems, traveling-wave regimes are possible, under which all Josephson junctions are under identical electrodynamic conditions and make coherent contributions to the radiation field. Such systems, which will be called active Josephson traveling wave antennas, are scalable, i.e., in the case of optimal matching, the intensity of their radiation increases in proportion to the size of the system or the number of the Josephson junctions. An important component, which ensures coherence of the contributions made by a great number of junctions, is the lateral energy leakage from the transmission line (vertical radiation output), which prevents saturation of the nonlinearity of individual junctions with narrow dynamic ranges. Such systems can be used as a basis for Josephson oscillators producing power levels sufficient for practical applications. A simple qualitative theory of open Josephson traveling-wave lines was developed and conditions for existence and stability of travelling wave regimes were found [1].

If there exists the traveling wave of current along Josephson array with wave number h it will radiate electromagnetic wave to open space at an angle $\alpha = \sin^{-1} h/k$, where k is the wave number of the emitted wave in vacuum and α counted from normal to substrate. For $h/k < 1$ when current wave is faster than speed of light in vacuum it is an ordinary transverse electromagnetic wave, for homogeneous current with $h = 0$ the radiation will be directed strictly vertical. But for $h/k < 1$ when current wave is slow the angle α is imaginary and the traveling electromagnetic wave turns to a surface plasmon traveling along the interface of the wafer and radiated from the edge of structure.

It should be noted that due to not perfect matching conditions at edges of array the traveling wave would not be pure traveling and some mixture of opposite propagating wave will always be presented. But Standing Wave Ratio (SWR) should be final to provide the absence of AC field nodes so that all junctions will be pumped by common field. Since the AC current distribution and radiated field defined by cooperative dynamics of Josephson junctions should be found self consistently we undertook direct computer simulations of such active Josephson antennae.

A numerical simulation code based on the Finite Difference Time Domain (FDTD) method and a self-consistent solution of the nonlinear equations which describe the Josephson junctions has been developed. The results of simulation of some variants of Josephson traveling-wave antennas with different radiation patterns are presented.

An example chosen for the calculations is a Josephson system similar to the two folded wire traveling-wave antenna. The simulated Josephson system is a set of thin perfect conductors, lumped linear elements, such as capacitors, inductances, resistors, and sources of DC electromotive forces, and nonlinear active elements, Josephson junctions simulated by resistively and capacitive shunted model. These elements are located on the surface of a dielectric plate and interact via the electromagnetic field in the surrounding space. Calculations start from an initial distribution for Josephson phases and electric and magnetic fields on the computational grid and continue until a stationary state is reached. After that time average values of voltages and currents in Josephson junctions and Fourier amplitudes of the fields around the sample are

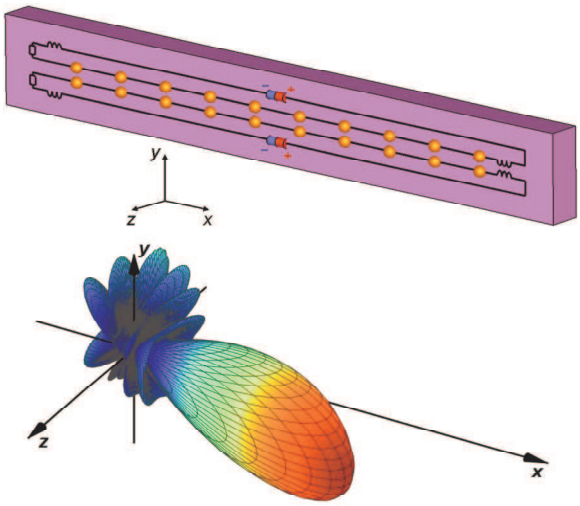

Fig. 1. Appearance and directivity pattern of two folded Josephson active antenna with separate DC bias demonstrating oblique angle radiation due to junction synchronization with fast traveling current wave. Yellow circles denote Josephson junctions, bias battery, resistor and inductances, serving for matching are denoted as usual.

obtained. The radiation pattern at a fixed frequency is calculated using a standard near-to-far field transformation [3]. Full power of emission was calculated by integration of the far field Pointing vector. Examples of such systems representing an antenna containing a set of straight and broken wires with different number of Josephson junctions imbedded into together with radiation patterns generated by them are shown on Fig. 1-3. The pictures shown demonstrate various regimes of radiation manifested itself by different radiation patterns which strongly depend on geometry of antennae and DC bias. When bias increases the oscillation frequency defined by Josephson relation $\hbar\omega = 2eV$ also increases, mode spectrum enriches and directivity patterns became more complicated. As it is common for oversized radiating system to control generation regimes and directivity pattern some complication of the system to provide working mode selection is needed. This work is now underway.

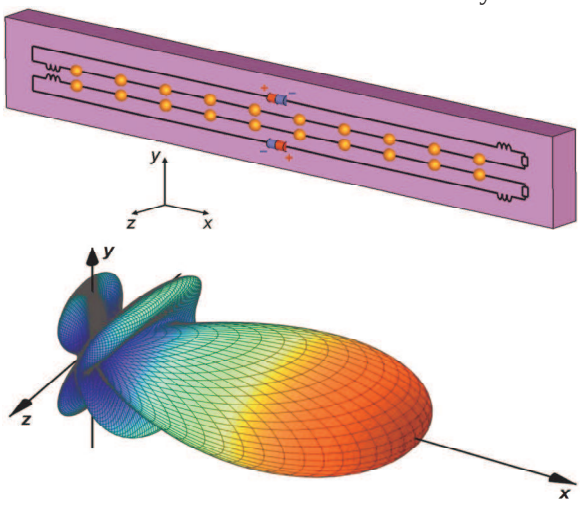

Fig. 2. The same Josephson active antenna as in Fig. 1 but radiated along the wafer due to synchronization with slow current wave.

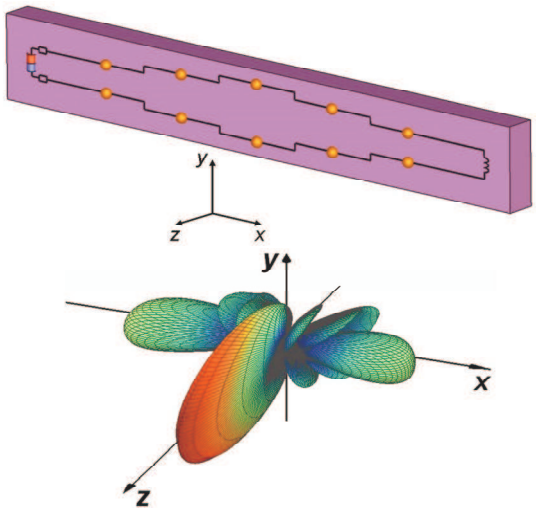

Fig. 3. Appearance and directivity pattern of Josephson active antenna consisting of two broken lines with common DC bias. It I seen pronounced lobe corresponding to vertical output of radiation due to junction synchronization with homogeneous mode of substrate.

Dependence of power of radiation and behavior of spectral properties of radiation on junction number, current and voltage spectra on individual junctions support suggested concept of array synchronization by traveling wave.

Recently [4] Josephson emission from such larger-than-the-wavelength Nb-NbSi-Nb junction arrays consisting of order 10^4 junctions was investigated experimentally and angular dependence of radiated energy was measured by small InSb semiconductor detector. The asymmetry of radiation pattern that was found support the suggested our concept of synchronization mediated by traveling wave. We argue that such a mechanism of synchronization opens a possibility for phase locking of very large arrays of oscillators what opens a way to develop effective Josephson oscillator of Terahertz range.

The work was supported by the Russian Foundation for Basic Research (Grants No. 18-02-00912), V. V. K. would also like to acknowledge the partial support of this research by the Russian Science Foundation (Grant No. 15-12-10020).

References

1. *V. V. Kurin, N.K.Vdovicheva, and I.A. Shereshevskii,* Josephson Traveling-Wave Antennas, Radiophysics and Quantum Electronics, **59**, 922, (2017)

2. *C. A. Balanis*, in Antenna Theory: Analysis and Design, 3rd ed. (Wiley Interscience, New York, 2005), Chap. 10.

3. A. *Taflove and S. C. Hagness*, in Computational Electrodynamics: The Finite-Difference Time-Domain Method, 3rd ed. (Artech House Inc., Boston and London, 2005), Chap. 8.

4. *M. A. Galin, E. A. Borodianskyi, V. V. Kurin, I. A. Shereshevskiy, N. K. Vdovicheva, V. M. Krasnov, A. M. Klushin,* Synchronization of Large Josephson-Junction Arrays by Traveling Electromagnetic Waves, Phys. Rev. Applied **9**, 054032 (2018)

Generation of THz radiation by photoconductive antennas on based thin films InGaAs and InGaAs/InAlAs.

A.A. Leontyev[1], K.A. Kuznetsov[1], G.B. Galiev[2], G.Kh. Kitaeva[1], V.V. Kornienko[1], E.A. Klimov[2], A.N. Klochkov[2], S.S. Pushkarev[2], and P.P. Maltsev[2]

[1] Lomonosov Moscow State University, Moscow 119991, Russia, aa.leontjev@physics.msu.ru
[2] Institute of Ultrahigh Frequency Semiconductor Electronics, RAS, Moscow 117105, Russia

Epitaxial low-temperature grown (LT) semiconductor arsenides (Al, Ga, In)As are widely used as materials for photoconductive antennas (PCA) generators and detectors of pulsed radiation in the terahertz (THz) frequency range [1–3]. It is the combination of subpicosecond carrier lifetime, relatively high mobility and high resistivity that makes LT-materials suitable for PCA applications. Lately, InGaAs has been investigated as a potential candidate for THz-PCA photoconductive material due to room-temperature band gap of 0.74 eV, which allows for 1.56 μm optical excitation with Er^{3+} fiber laser femtosecond pulses [4–6].

The low substrate temperatures result in a non-stoichiometric growth with the incorporation of excess arsenic in the crystal structure. The most common non-stoichiometry-related point defects in LT-arsenides are arsenic antisites with concentrations in the range 10^{17}–10^{19} cm^{-3} depending on the substrate temperature and arsenic overpressure [7–10]. Antisite-related defect band in the semiconductor energy bandgap play a significant role in carrier dynamics. Fast non-radiative recombination of photogenerated electrons and holes through antisite centers results in sub-picosecond carrier lifetimes in LT-materials at optimized growth and annealing conditions [11, 12]. It is generally agreed that main traps of photo-excited electrons are ionized antisite defects [13–15].

A possible approach to increase the resistivity of LT-InGaAs structures is to employ LT-InGaAs/InAlAs superlattices [6,13,16,17]. LT-InAlAs layers have a higher dark resistivity as compared to LT-InGaAs and exhibit deep trap states that are situated energetically below the antisite defect levels of adjacent InGaAs layers that results in a reduction of residual carrier concentration.

The Fig.1 shows the amplitude of THz radiation in time domain. It is seen that the signal from an InGaAs /InAlAs-based structure is 5-6 times higher due to a higher bias voltage, which is possible (without sample breakdown) due to higher sample resistance and lower dark current.

Fig.2 shows a comparison of the Fourier amplitude according to the materials of the antennas LT-InGaAs/InAlAs and LT-InGaAs. It is seen that the spectrum of the LT-InGaAs / InAlAs sample is slightly wider in the range from 0.1 THz to 0.6 THz than that of the LT-InGaAs sample. We explain this effect by the difference between the characteristic relaxation times of electrons in the transition from the conduction band to the antisites.

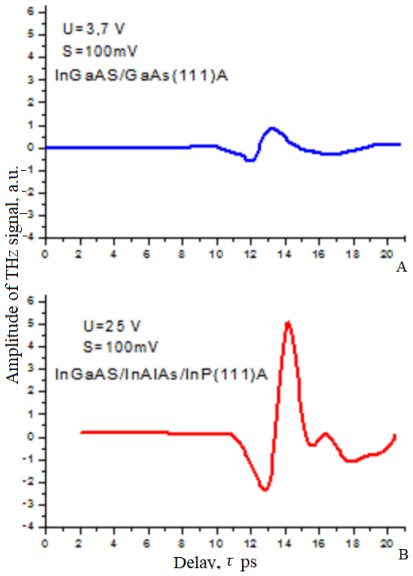

Fig.1. Time-domain waveforms detected for the following antenna materials: A) LT-InGaAs B) LT-InGaAs/InAlAs.

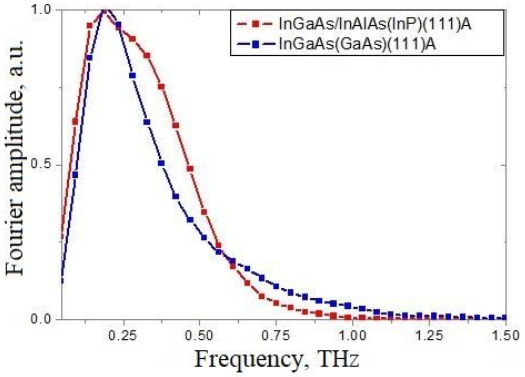

Fig. 2. Compare spectral amplitudes by antenna materials LT-InGaAs(Blue line), LT-InGaAs/InAlAs (Red line).

We determined the characteristic times of electron relaxation by the "pump-probe" spectroscopy method. Fig.3 shows the dependence of the normalized transmission in time domain for the samples of LT-InGaAs and LT-InGaAs / InAlAs.We used 2-exponentional model for description experimental curves. On figures τ_1 is an electron capture time (capture by charge As_{Ga} defects) [18,19], τ_2 is a recombination time of captured electrons and holes [17].

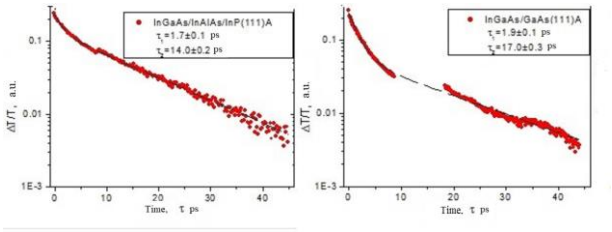

Fig. 3 Change the transmission coefficient in the time domain.

Due to the experimental fact that the characteristic relaxation times for the LT-InGaAs / InAlAs sample are less than for the LT-InGaAs, we observed the difference in the spectra for these samples.

Summing up, it was found that THz generation is about 5-6 times more efficient in the case of LT-InGaAs/InAlAs superlattice than LT-InGaAs generation. It is found that due to the shorter electron relaxation time in the superlattice, the spectrum of these samples is wider in the range of 0.1-0.6 THz.

This study was performed under the support of the RFBR grant № 16-02-258a.

References

1. *G.Kh. Kitaev.a* Terahertz generation by means of optical lasers // Laser Phys. Lett. V. 559, P. 20085.
2. *N.M. Burford and M.O. El-Shenawee.* Review of terahertz photoconductive antenna technology // Opt. Eng. 2017, V. 56, P. 10901.
3. *E. Castro-Camus and M. Alfaro.* Photoconductive devices for terahertz pulsed spectroscopy: a review // Photon. Res. 2016, V. 4, P. A35.
4. *A. Takazato M. Kamakura, T. Matsui,J. Kitagawa and Y. Kadoya.* Terahertz wave emission and detection using photoconductive antennas made on low-temperature-grown InGaAs with 1.56 μm pulse excitation // Appl. Phys.Lett. 2007, V. 91, P. 011102.
5. *I. Kostakis and M. Missous.* Optimization and temperature dependence characteristics of low temperature $In_{0.3}Ga_{0.7}As$ and $In_{0.53}Ga_{0.47}AsIn_{0.52}Al_{0.48}As$ semiconductor terahertz photoconductors // AIP Adv. 2013. V. 3, P. 092131.
6. *B. Sartorius, H. Roehle, H. Künzel, J. Böttcher, M. Schlak, D. Stanze, H. Venghaus and M. Schell.* All-fiber terahertz time-domain spectrometer operating at 1.5 μm telecom wavelengths Opt. Express 2008, 16 9565
7. *X. Liu, A. Prasad, J. Nishio, E.R. Weber, Z. Liliental-Weber and W. Walukiewicz.* Native point defects in low-temperature-grown GaAs // Appl. Phys. Lett. 1995. V. 67, P. 279.
8. *H. Künzel, J. Böttcher, R. Gibis and G. Urmann* Material properties of $Ga_{0.47}In_{0.53}As$ grown on InP by low-temperature molecular beam epitaxy // Appl. Phys. Lett. 1992. V. 61, P. 1347.
9. *R.A. Metzger, A.S. Brown, L.G. McCray and H.A. Henige.* Structural and electrical properties of low temperature GaInAs // J. Vac. Sci. Tech. B. 1993. V. 11, P. 798.
10. *M.R. Melloch, J.M. Woodall, E.S. Harmon, N. Otsuka, F.H. Pollak, D.D. Nolte, R.M. Feenstra and M.A. Lutz.* Low-temperature grown III-V materials // Annu. Rev. Mater. Sci. 1995. V. 25, P. 547.
11. *C. Baker, I.S. Gregory, W.R. Tribe, I.V. Bradley, M.J. Evans, E.H. Linfield and M. Missous.* Highly resistive annealed low-temperature-grown InGaAs with sub-500fs carrier lifetimes // Appl. Phys. Lett. 2004. V. 85, P. 4965.
12. *K.A. McIntosh, K.B. Nichols, S. Verghese and E.R. Brown.* Optical and terahertz power limits in the low-temperature-grown GaAs photomixers // Appl. Phys. Lett. 1997, V. 70, P. 354.
13. *B. Globisch, R.J.B. Dietz, D. Stanze, T. Göbel and M. Schell.* Carrier dynamics in beryllium doped low-temper-ature-grown InGaAs/InAlAs // Appl. Phys. Lett. 2014. V. 104, P. 172103.
14. *Z. Liliental-Weber, H.J. Cheng, S. Gupta, J. Whitaker, K. Nichols and F.W. Smith.* Structure and carrier lifetime in LT-GaAs // J. Electron. Mater. 1993. V. 22, P. 1465.
15. *U. Siegner, R. Fluck, G. Zhang and U. Keller.* Ultrafast high-intensity nonlinear absorption dynamics in low-temperature grown gallium arsenide // Appl. Phys. Lett. 1996. V. 69, P. 2566.
16. *H. Kuenzel, K. Biermann, D. Nickel and T. Elsaesser.* Low-temperature MBE growth and characteristics of InP-basedAlInAs/GaInAs MQW structures // J. Cryst. Growth. 2001. V. 284, P. 227
17. *R.J.B. Dietz, B. Globisch, H. Roehle, D. Stanze, T. Göbel and M. Schell.* Influence and adjustment of carrier lifetimesin InGaAs/InAlAs photoconductive pulsed terahertz detectors: 6 THz bandwidth and 90dB dynamic range // Opt.Express. 2014. V. 22, P. 19411.
18. *C. Baker, I.S. Gregory, W.R. Tribe, I.V. Bradley, M.J. Evans, E.H. Linfield and M. Missious.* Highly resistive annealed low-temperature-grown InGaAs with sub-500 fs carrier lifetimes // Appl. Phys. Lett. 2004, V. 85, P. 4965.
19. *B. Globisch, R. Dietz, R. Kohlhaas, T. Göbel, M. Schell, D. Alcer, M. Semtsiv, and W. Masselink.* Iron doped InGaAs: Competitive THz emitters and detectors fabricated from same photoconductor. // J. Appl. Phys. 2017. V. 121, P. 053102.

High Photoconductivity in Heavily Doped GaAs/AlAs Superlattices with Electric Domains

S. K. Paprotskiy[1], I. V. Altukhov[1], M. S. Kagan[1], N. A. Khvalkovskiy[1], I. S. Vasil'evskii[2], A. N. Vinichenko[2]

[1]V.A. Kotel'nikov Institute of Radio Engineering and Electronics, Russian Ac. Sci., Moscow, Russia, s.paprotskiy@gmail.com

[2]National Research Nuclear University MEPhI, Moscow, Russia

In last three decades, the electron transport in semiconductor superlattices (SLs) has been studied in detail [1, 2], mainly in connection with the predicted amplification of Bloch waves, which can make it possible to create tunable sources of THz radiation. The main hindrance to the Bloch wave amplification is the formation of electrical domains owing to the static negative differential conductivity (NDC) arising in superlattices at resonant tunneling between confined states in neighboring quantum wells. Many works were devoted also to studies of domain properties (see, e.g., [2] and references therein). Most of them were performed with weakly doped SLs at low temperatures under strong illumination [2-7]. The change in free carrier concentration under illumination gives rise to different domain regimes. It has been shown, in particular, that transition from travelling to static domain regime occurs at sufficiently high illumination intensity. In this work studies of effect of interband illumination on tunneling current in highly doped short-period superlattices at the domain formation are presented.

We used the MBE grown GaAs/AlAs SLs consisted of 100 periods of 4 nm GaAs/2 nm AlAs between heavily doped (~10^{19}cm^{-3}) n^+ cap layer and n^+ substrate. GaAs quantum wells (QWs) were Si doped with concentration of $2*10^{17}$cm^{-3}. A cross-section of the structure is shown in Fig. 1.

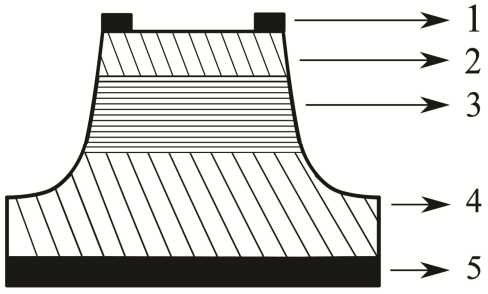

Fig. 1. Scheme of the structure: (*1*, *5*) top and bottom metal contacts, (*2*) top contact n^+ layer, (*3*) superlattice, and (*4*) heavily doped substrate.

Triangular voltage pulses with sweep-up times of 0.2 to 10 μs and sweep-down times up to 100 μs were used to record I-V curves. Measurements were performed at room temperature.

A sharp decrease of current at some threshold voltage (Fig. 2) indicates the moving domain formation. The current rise in the mean is an evidence of triangular form of the domain [2, 9]. The series of maxima in current-voltage characteristics is attributed to the optical phonon assisted tunneling between quantum wells inside the triangular domain.

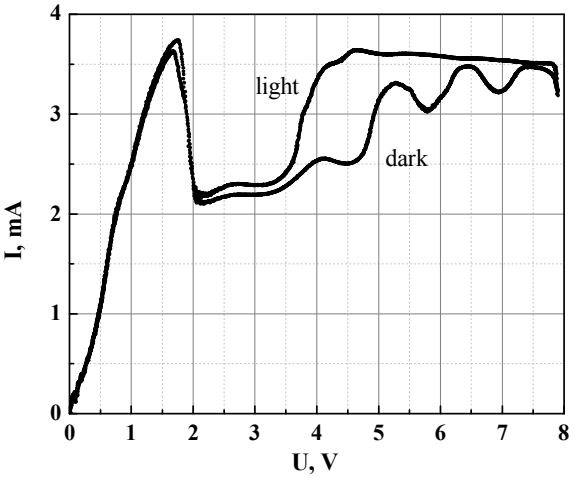

Fig. 2. Current–voltage characteristics of the GaAs/AlAs SL in the dark (lower curve) and under band-to-band illumination (upper curve).

A strong effect of rather weak illumination (with a LED or a filament bulb) on a tunneling current in GaAs/AlAs SLs with relatively high doping level was found under conditions of electric domains formation. Fig. 2 shows the current-voltage characteristics with and without illumination. The photocurrent at the domain regime could reach 50% of the dark current, while it was several orders of magnitude less at voltages below the threshold one (before the domain formation) as the free carrier concentration excited with light was considerably less than Si donor concentration. The measured photocurrent spectrum (Fig. 3) points to the band-to-band excitation. The spectral long-wavelength cutoff allows us to determine the GaAs QW gap and the energy of first size quantization level. These energies coincide with known values for GaAs QW.

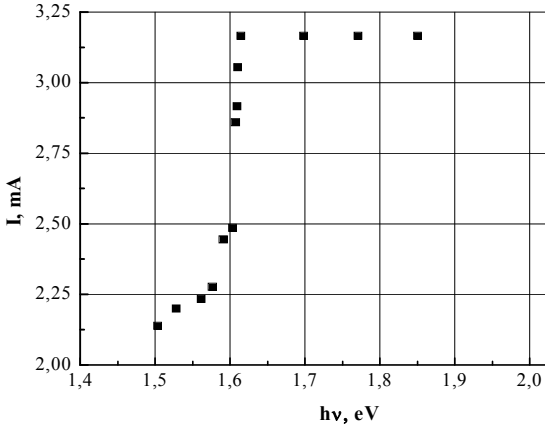

Fig. 3. Photocurrent spectrum

The large photocurrent at the domain formation is referred to the triangular form of high-field domain with wide region of donor depopulation. The free carrier concentration in this region is very small and additional concentration of electron-hole pairs created by interband illumination exceeds significantly a stationary concentration inside the domain, which results in a change of space charge at domain boundaries. This leads to a change of domain movement regime.

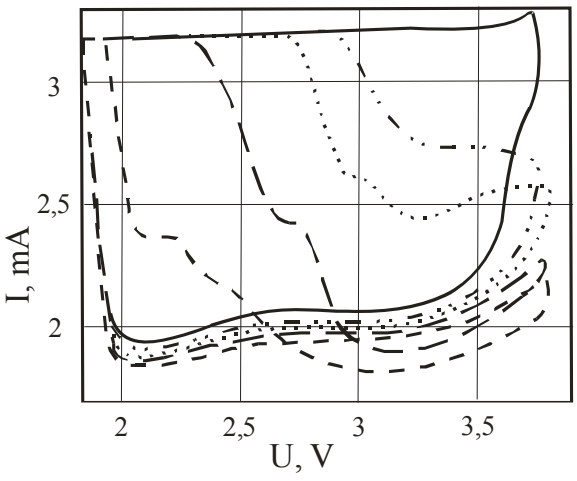

Fig. 4. Parts of current–voltage characteristics of the GaAs/AlAs SL in an intermediate range of domain existence at different light intensities.

The sufficiently intense illumination could initiate the travelling-to-static domain transition, which becomes apparent in current saturation regions in I-V curves (Fig. 2). Shown in Fig. 4 are parts of current-voltage characteristics corresponding to an intermediate voltage range of domain existence for different illumination intensities. I-V curves were measured at forward and backward bias sweep. The current hysteresis is connected with a large asymmetry of transition times from moving to static field domain and back at voltage sweep-up and sweep-down, respectively [10]. In this voltage range (compare with Fig. 2), the current saturation was observed only at backward voltage sweep.

The work was supported by RFBR grants 16-29-03135 and 16-29-09626

References

1. *Wacker, A.* Semiconductor superlattices: a model system for nonlinear transport // Physics Reports, 2002. V. 357, P. 1

2. *Bonilla, L. L., Grahn H. T.* Non-linear dynamics of semiconductor superlattices // Rep. Prog. Phys. 2005. V. 68, No. 3, P. 577

3. *Sun B. Q., Jiang D. S. and Wang X. J.* Current oscillations and stable electric field domains in doped GaAs/AlAs superlattices // *Semicond. Sci. Technol.* 1997, V. 12**,** No 4, P. 401

4. *Tomlinson A. M., Fox A. M., Cunningham J. E. and Jan W. Y.* Photocurrent self-oscillations in a spatially direct GaAs/AlGaAs superlattice // Appl. Phys. Lett. 1999, V. 75, P. 2067

5. *Kwok S. H., Grahn H. T. et al.* Nonresonant carrier transport through high-field domains in semiconductor superlattices // Phys. Rev. B. 1995. V. 51. P. 9943

6. *Kwok S. H., Norris T. B., Bonilla, L. L.,et al.* Domain-wall kinetics and tunneling-induced instabilities in superlattices // Phys. Rev. B 1995. V. 51. P. 10171

7. *Grahn H. T., Schneider H., v. Klitzing K.* Optical studies of electric field domains in GaAs/$Al_xGa_{1-x}As$ superlattices // Phys. Rev. B 1990. V. 41, P. 2890

8. *Ohtani N., Egami N., Grahn H. T., Ploog K. H., and Bonilla L. L.* Transition between static and dynamic electric-field domain formation in weakly coupled GaAs/AlAs superlattices // Phys. Rev. B 1998. V. 58, P. R7528(R)

9. *Suris R. A.* Inhomogeneous structures in semiconductors with superlattices // Sov. Phys. Semicond. 1973. V. 7, No. 8, P. 1035

10. *Altukhov I. V., Kagan M. S., Paprotskiy S. K., Khvalkovskiy N. A., Vasil'evskii I. S., Vinichenko A. N.* Electronic Tunneling and Electric Domains in GaAs/AlAs Superlattices at Room Temperature, this issue.

Plasmonic terahertz antennas with high-aspect ratio metal gratings

A.E. Yachmenev[1,2], D.V. Lavrukhin[1,2], I.A. Glinskiy[1,2], R.A. Khabibullin[1,2,3], R.R. Galiev[1], A.Yu. Pavlov[1,2], Yu.G. Goncharov[2], I.E. Spektor[2], M. Ryzhii[5], T. Otsuji[6], K.I. Zaytsev[2,4] and D.S. Ponomarev[1,2,3]

[1]Institute of Ultra High Frequency Semiconductor Electronics of RAS, Moscow, Russia, ponomarev_dmitr@mail.ru
[2]Prokhorov General Physics Institute of RAS, Moscow, Russia
[3]Center for Photonics and 2D Materials, Moscow Institute of Physics and Technology, Dolgoprudny, Russia
[4]Bauman Moscow State Technical University, Moscow, Russia
[5]Department of Computer Science and Engineering, University of Aizu, Aizu-Wakamatsu, Japan
[6]Research Institute of Electrical Communication, Tohoku University, Japan

The state-of-art terahertz (THz) emitters and detectors are of great interest due to its wide applications in security systems, biology, medicine and material science [1–3]. Despite the variability of existing THz generation principles photoconductive antenna (PCA) is still promising THz emitter for broadband THz spectroscopy and imaging. Since its first demonstration by Auston's research on silicon substrate [4], numerous studies have been carried out. Despite the considerable progress in developing PCAs there are still challenges such as increasing an emitted THz power, an optical-to-THz conversion efficiency, a bandwidth of a PCA and its thermal stability.

In present article, we present a novel technology with a passivation approach for fabricating a dielectric-filled plasmonic PCA that allows us for reaching a 100 nm-height plasmonic gratings and strongly reduce leakage currents. In the proposed technology two different dielectrics are separately used: a Si_3N_4 for preliminary passivating a surface of a photoconductor to reduce a dark current flow and Al_2O_3 dielectric for filling and covering plasmonic gratings to increase an incident light coupling. This approach allows for sustaining a thermal stability of a PCA and is suitable for any photoconductive material, due to excluding a mesa etching, which is of particular importance for InGaAs-based PCAs.

It is well known that all types of PCAs, especially the log-periodic and log-spiral antennas, suffer from high leakage currents, because a dark current flows between the full length of the antenna bias lines which is hundred times longer than the optical excitation spot. In order to significantly decrease a dark current flow we have developed a novel technology for a PCA fabrication where an antenna metallization, including contact pads, is deposited on a photoconductor's surface preliminary covered (i.e. passivated) with a dielectric through etched windows. The schematic layout of the proposed PCA is depicted in Fig. 1.

Prior to fabrication process we carried out numerical calculations by means of a 2D finite element method-based solver for analyzing the interaction between a TM-polarized laser pump beam and plasmonic gratings. The calculation domain consisted of 4 periods of plasmonic gratings (4×200 nm) with width and distance between them equal to 100 nm, deposited on 3-μm GaAs substrate. First, we calculated an electric field near plasmonic gratings distribution versus a height (h) of metal gratings which showed that an increase of metal height leads to a continuous enhancement of an electric field and its maximum is shifted toward high values of h, which is difficult to being experimentally achieved according to chosen high aspect-ratio of gratings, which is defined as the ratio between a width of a grating to its period.

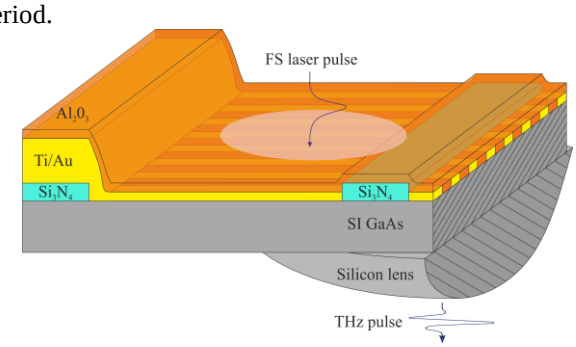

Fig. 1. Schematic layout and operation principle of the proposed dielectric-filled plasmonic THz emitter with high-aspect ratio metal gratings. A lower dielectric Si_3N_4 layer is used for reducing leakage currents (to sustain a thermal stability enhancement) while an upper Al_2O_3 dielectric serves for filling a distance between gratings and covering them to increase an incident light confinement. Also it acts as an anti-reflection coating layer

Thus we considered the case of h = 100 nm with aspect-ratio equal to 0.5, that to our knowledge has not been reached experimentally yet. Second, we estimated an optimum thickness of Al_2O_3 dielectric layer which entirely fills a distance between gratings to enhance a light coupling and simultaneously mitigate the Fresnel reflection losses for the case of h = 100 nm. We demonstrated that the dependency of an incident laser pump reflection coefficient on Al_2O_3 thickness (d) has a minimum which corresponds to 180 nm thickness of Al_2O_3. Afterwards, when fabricating the PCA, we used these parameters of the dielectric thickness and plasmonic gratings height, i.e. d = 180 nm and h = 100 nm, respectively.

Figure 2 shows scanning electron microscope (SEM) image of the fabricated dielectric-filled plasmonic PCA with log-spiral topology and a magnified image of plasmonic gratings. Initially we passivated GaAs photoconductor's surface by 230 nm Si_3N_4 dielectric, where the windows for 50/450 nm Ti/Au antenna electrodes were etched. Therefore antenna electrodes were deposited on a photoconductor's surface only through the etched windows in Si_3N_4 while a PCA's gap remained passivated. Plasmonic gratings were formed by electron-beam lithography with 18/75

nm Ti/Au metallization followed by lift-off. The PCA fabrication is partially described in Refs. [5,6].

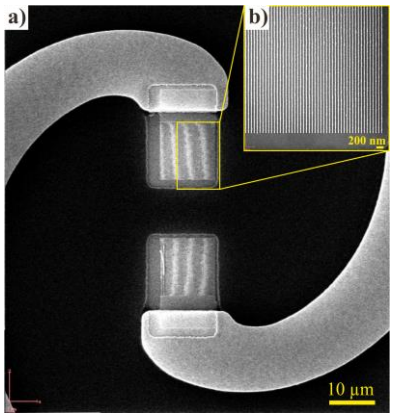

Fig. 2. SEM image of the fabricated plasmonic PCA (a) with a magnified image of plasmonic gratings (b)

The experimentally-measured current-voltage characteristics without laser illumination (see Fig. 3) demonstrated significant reduction of a dark current when a surface of GaAs is passivated by Si_3N_4 in comparison to a non-passivated one (more than three orders of a magnitude) demonstrating that the selected size of window in Si_3N_4 leads to strong decrease of a dark current, keeping a transient photocurrent remained.

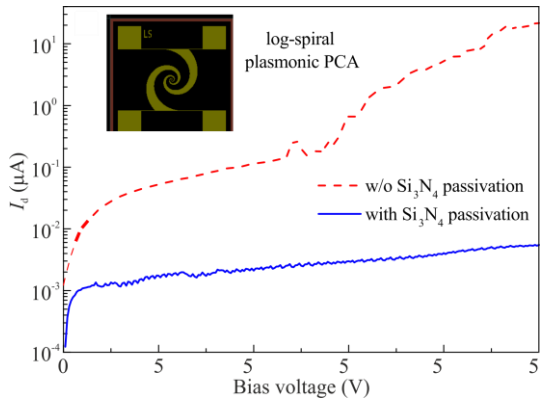

Fig. 3. Current-voltage characteristics without laser illumination measured for the proposed PCA when using Si_3N_4 dielectric (solid line) and without it (dashed line)

In order to demonstrate a performance of the proposed PCA we examined it by means of THz time-domain spectroscopy and compared to the traditional one. The both PCAs were used as a THz emitter, while compact all-fiber-based Toptica FemtoFErb780 laser was used as pump source with mean power up to 10 mW with a bias voltage equal to 30 V. As seen in Fig. 4 the spectra shape remain unchanged for the both PCAs, but the proposed PCA demonstrates 2000-100 times increase of the emitted THz power depending on laser pump (not attached in this article). Since PCAs are saturated at high laser pump due to electric field screening, we additionally investigated the emitted THz power versus laser pump in order to find out an optimum illumination regime. We showed that the transient photocurrent for the proposed and traditional PCAs is trending to converge at laser pump close 10 mW, though at low pump energies the transient photocurrent generated by the proposed PCA is up to 25 times higher than for the traditional one.

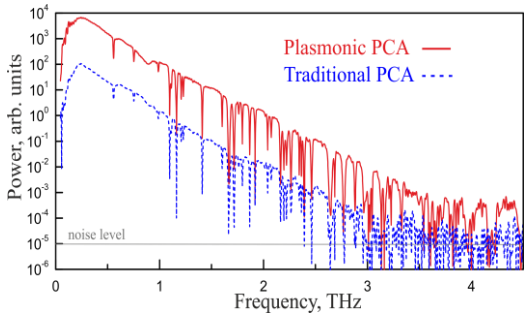

Fig. 4. Radiated THz power in the frequency-domain for the plasmonic and traditional PCAs based on SI-GaAs photoconductor

The work was supported by the Russian Scientific Foundation (Project No.18-79-10195) and RIEC ICRP (grant H30/A04). The numerical simulation of the PCA under consideration was supported by the President's grant of Russian Federation for young scholars (Project MK-5450.2018.2).

References

1. *Yardimci N., Cakmakyapan S., Hemmati S., Jarrahi M.* A high-power broadband terahertz source enabled by three-dimensional light confinement in a plasmonic nanocavity // Sci. Rep. 2017. V. 7. P. 4166.

2. *Ponomarev D. S., Lavrukhin D. V., Yachmenev A. E., Khabibullin R. A, Semenikhin I. E., Vyurkov V. V., Ryzhii M., Otsuji T., Ryzhii V.* Lateral terahertz hot-electron bolometer based on an array of Sn nanothreads in GaAs // J. Phys. D: Appl. Phys. 2018. V. 51. P. 135101.

3. *Ryzhii V., Ryzhii M., Svintsov D., Leiman V., Maltsev P., Ponomarev D., Mitin V., Shur M., Otsuji T.* Real-space-transfer mechanism of negative differential conductivity in gated graphene-phosphorene hybrid structures: Phenomenological heating model // arXiv: 2018. 1806.06227.

4. *Auston D.* Picosecond optoelectronic switching and gating in silicon // Appl. Phys. Lett. 1975. V. 26. P. 101.

5. *Ponomarev D.S., Khabibullin R.A., Yachmenev A.E., Pavlov A.Yu., Slapovskiy D.N., Glinskiy I.A., Lavrukhin D.V., Ruban O.A., Maltsev P.P.* Electrical and thermal properties of photoconductive antennas based on $In_xGa_{1-x}As$ (x>0.3) with a metamorphic buffer layer for the generation of terahertz radiation // Semicond. 2017. V. 51(9). P. 1218–1223.

6. *Lavrukhin D. V., Katyba G. M, Yachmenev A. E., Galiev R. R., Glinskiy I. A., Khabibullin R. A., Goncharov Yu. G., Spektor I. E., Khusyainov D. I., Buryakov A. M., Mishina E. D., Chernomyrdin N. V., Zaytsev K. I., and Ponomarev D. S.* Numerical simulations and experimental study of terahertz photoconductive antennas based on GaAs and its ternary compounds // Proc. SPIE 10680. 2018. V. 106801M.

Doubling of gyrotron radiation frequency due to nonlinear susceptibility in A3B5 semiconductors

Vladimir V. Rumyantsev[1], A. A. Dubinov[1], A.P. Fokin[2], V.V. Utochkin[1], M.Yu. Glyavin[2], S. V. Morozov[1]

[1]Institute for Physics of Microstructures of RAS, Nizhny Novgorod, Russian Federation, rumyantsev@ipmras.ru
[2]Institute of Applied Physics of RAS, Nizhny Novgorod, Russian Federation

At present, there is much activity aimed for development and application of different sources of radiation with terahertz (THz) frequency range, which are necessary for a variety of scientific and practical applications such as spectroscopy, radioastronomy, environmental monitoring, security and counter-terrorism [1]. Powerful sources of THz radiation like synchrotrons and free electron lasers (FELs) have high cost and large size, which limits their use even for scientific applications. Complicated solutions are required to increase the frequency of the vacuum sources such as a backward wave oscillator up to 1 THz and higher [2]. Semiconductor quantum cascade lasers in THz range operate only at cryogenic temperatures [3-5]. Molecular lasers, although operating at room temperature, are available only for a fixed set of frequencies [6]. THz radiation sources based on femtosecond lasers exhibit an extremely broad spectrum (~1 THz wide), which is not always acceptable for spectroscopy applications and have rather low output power [7]. Currently, the media of choice for optical rectification are LiNbO3 [8], ZnTe [9], GaP [10] crystals. They all have fairly high losses in the THz range and the conversion efficiency even for state-of-the-art experiments is approaching 10^{-3} [8] and in typical cases is an order of magnitude lower.

Alternative way to obtain intense THz radiation is to "multiply" the frequency of incident radiation using nonlinear susceptibility in semiconductors. This approach requires intense sources at the fundamental frequency in sub-THz range, among which there were mainly molecular lasers. However, recently a sufficient progress has been made in the development of sub-THz range gyrotrons. Continuous wave (cw) gyrotrons with frequencies of 460 GHz [11] and 527 GHz [12] have been demonstrated. IAP RAS recently developed unique pulse solenoids with magnetic fields up to 50 T that allowed implementing gyrotrons on the first cyclotron harmonic with the output frequency of up to 1.3 THz with pulse duration ~ 50 μs [13]. On the basis of "dry" cryomagnet with magnetic fields up to 10 T cw gyrotrons with frequencies 263 GHz [14] and 250 GHz were fabricated. A generator with 889 GHz frequency (in a synchronism with the third harmonic of the cyclotron frequency) was developed, as well as a pulsed generator with a frequency of ~1THz and power of ~10 W at the second harmonic of gyrofrequency [15]. These results were obtained by using the unique cryomagnet with the magnetic field of up to 20 T. In 2017, a double-beam gyrotron at the second harmonic with frequency of 0.8 THz was demonstrated [16].

For such sources, frequency doubling is enough to obtain frequencies above 1 THz, while previous works focused on generating the third harmonic of gyrotron radiation in n-type Ge and Si at much lower frequencies [17, 18]. Third harmonic generation was demonstrated in Ref. [17] with the effectiveness of 0.05% under gyrotron pumping with 70 GHz frequency, and in Ref. [18] under gyrotron pumping with 118 GHz frequency and 0.07% conversion efficiency. The frequency tripling is possible in semiconductor materials due to the third order nonlinearity, which is predominantly electronic (third order nonlinearity due to ionic motions is usually weaker) [19, 20]. The frequency doubling is possible in crystals lacking the inversion centre. In this work we consider the prospects of several A3B5 semiconductors for frequency doubling due to the second order susceptibility of the crystal lattice. It should be noted that nonlinear optical properties of A3B5 materials have been quite poorly studied in far infrared region where the frequency dispersion of second order nonlinear coefficient is substantial [21 - 24]. Second-order susceptibility and corresponding frequency doubling were investigated mainly in GaAs, using CH_3F laser [21] and free electron laser [22] as the radiation sources in the spectral ranges of 0.6 - 1.7 THz and 4 -- 6 THz, respectively. However, second order nonlinearity in GaAs is rather weak as can be seen from table:

Table. Second-order susceptibility of several A3B5 semiconductors

Semiconductor	Second-order susceptibility, χ [21, 25]
GaAs	$57 \cdot 10^{-10}$ cm/V
GaP	$18 \cdot 10^{-10}$ cm/V
GaSb	$150 \cdot 10^{-10}$ cm/V
InP	$345 \cdot 10^{-10}$ cm/V
InAs	$155 \cdot 10^{-10}$ cm/V
CdTe	$100 \cdot 10^{-10}$ cm/V [26]

The intensity of the second harmonic $I_{2\upsilon}$ can be calculated [27] as (c -- light velocity, n(υ) -- refractive index at the frequency υ, Δn = n(υ) - n(2υ))

$$I_{2\nu} = \frac{128\pi^5 \chi^2 \nu^2 L^2}{n(\nu)^2 n(2\nu) c^3} I_\nu^2 \left(\frac{\sin 2\pi\nu\Delta nL/c}{2\pi\nu\Delta nL/c} \right)^2$$

Thus, the output intensity is proportional to the square of intensity at the fundamental frequency I_υ susceptibility χ, fundamental frequency υ and sample length L. As can been seen from the Table, the susceptibility in InP is 6 times higher than in GaAs, al-

lowing sufficient enhancement of the second harmonic intensity. Note that maximum crystal length can be limited by refractive index dispersion and the optical losses. Typical frequencies of the lattice vibrations of optical transitions related to impurity absorption are considerably higher than 1 THz in semiconductors under consideration [25]. Therefore, the losses are mainly due to free carriers, density of which can be made negligibly low in state-of-the-art InP, reducing the absorption coefficient in the 200 -- 800 GHz region down to less than 1 cm^{-1} [28]. The refractive index change with frequency in the same range is extremely small $\Delta n \sim 0.002$ [28]. Thus, the crystal of several cm length can be used for frequency doubling. Fig. 1 gives the comparison of estimated output power of the second harmonic for GaAs and InP with L = 5 cm and fundamental radiation power of 50 kW/cm^2.

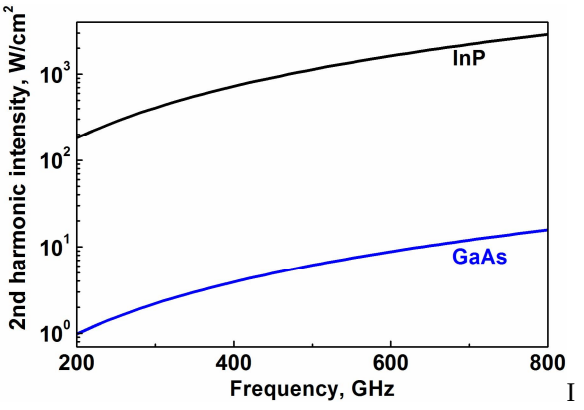

Fig. 1. The estimated second harmonic intensity vs. fundamental frequency for 5 cm long GaAs and InP crystals under fundamental radiation power of 50 kW/cm^2. Data on the refractive index for InP and GaAs is taken from Ref [28] and Ref [25], respectively

As can be seen, InP crystal is expected to provide about two-order enhancement over GaAs, studied in previous works [21-23]. We conclude that employing high-resistivity InP crystals is a promising route to obtain THz radiation by doubling the frequency of intense gyrotron radiation. The work was supported by Russian Science Foundation grant #18-79-10112.

References

1. *Van der Weide D.* Applications and Outlook for Electronic Terahertz Technology // Optics & Photonics News. 2003. V.14. No.4. P. 48-53

2. *Xiong Xu, Yanyu Wei, Fei Shen, Hairong Yin, Jin Xu et al.* A watt-class 1-THz backward-wave oscillator based on sine waveguide // Phys. Plasmas. 2012. 19, 013113.

3. *Williams B.S.* Terahertz quantum-cascade lasers // Nature Photonics. 2007. V.1. P. 517.

4. *Fathololoumi S., Dupont E., Chan C.W.I., Wasilewski Z.R., Laframboise S.R., Ban D., Matyas A., Jirauschek C., Hu Q., Liu H.C.* Terahertz quantum cascade lasers operating up to ~ 200 K with optimized oscillator strength and improved injection tunneling // Optics Express. 2012. 20 (4). 3866.

5. *Wang X., Shen C., Jiang T., Zhan Zh., Deng Q., Li W., Wu W., Yang N., Chu W., Duan S.*. High-power terahertz quantum cascade lasers with 0.23 W in continuous wave mode. // AIP Advances. 2016. 6. 075210.

6. *Dodel G.* On the history of far-infrared (FIR) gas lasers: Thirty-five years of research and application // Infrared Phys. Technol. 1999. 40 127–39

7. *Lewis R.A.* A review of terahertz sources // J. Phys. D: Appl. Phys. 2014. 47 374001

8. *Sergey B. Bodrov, Aleksey A. Murzanev, Yury A. Sergeev, Yury A. Malkov, and Andrey N. Stepanov* Terahertz generation by tilted-front laser pulses in weakly and strongly nonlinear regimes // Applied Physics Letters. 2013. 103. 251103

9. *Vidal S., Degert J., Tondusson M., Freysz E., and Oberlé J.*, Optimized terahertz generation via optical rectification in ZnTe crystals // J. Opt. Soc. Am. B. 2014. 31, 149-153.

10. *Taniuchi T., Nakanishi H.* Collinear phase-matched terahertz-wave generation in GaP crystal using a dual-wavelength optical parametric oscillator // Journ. Appl. Phys. 2004. v. 95, 7588.

11. Torrezan A.C., Han S.T., Mastovsky I., Shapiro M.A., Sirigiri J.R., Temkin R.J., Griffin R.G., Barnes A.B. Continuous-Wave Operation of a Frequency-Tunable 460-GHz Second-Harmonic Gyrotron for Enhanced Nuclear Magnetic Resonance. // IEEETrans. 2010. V.PS-38. №6.P.1150

12. Jawla S., Nanni E., Shapiro M. et al.// 2011 36th Int. Conf. on Infrared, Millimeter and Terahertz Waves (IRMMW-THz). Houston. 2-7 Oct. 2011. N.Y.IEEE, 2011. P. DOI 10.1109. IRMMWTHz.2011.61 05096

13. Glyavin M.Yu., Ginzburg N.S., Goldenberg A.L., Denisov G.G., Luchinin A.G., Manuilov V.N., Zapevalov V.E., Zotova I.V. THz Gyrotrons: Status and Possible Optimizations // Terahertz Science and Technology, V.5, No.2, 2012

14. Glyavin M. Yu., Chirkov A.V., Denisov G.G., et al. Experimental tests of a 263 GHz gyrotron for spectroscopic applications and diagnostics of various media. // Review of Scientific Instruments. 2015. 86. 054705.

15. Idehara T., Saito T., Ogawa I. The potential of the gyrotrons for development of the sub-terahertz and the terahertz frequency range — A review of novel and prospective applications, Proceedings of 2nd International Symposium on the Manipulation of Advanced Smart Materials // ThinSolidFilms. 2008. V. 517. No 4. P.1503, 2008

16. Idehara T., Glyavin M., Kuleshov A., Sabchevski S., Manuilov V., Zaslavsky V., Zotova I., Sedov A. A novel THz-band double-beam gyrotron for high-field DNP-NMR spectroscopy. // Rev.of Sci.Instrum. 2017. 88. 094708.

17 Keilmann F., Brazis R., Barkley H., Kasparek W., Thumm M. and Erckmann V. Millimeter-Wave Frequency Tripling in Bulk Semiconductors // EPL (Europhysics Letters), Volume 11, Number 4, p. 337

18 Narkowicz R., Siegrist M.R., Moreau Ph., Hogge J.P., Raguotis R. and Brazis R. Third-Order Susceptibility of Silicon Crystals Measured with Millimeter-Wave Gyrotron // Acta Physica Polonica A. 2011. V. 119, No. 4, p. 509

19. *Seeger K.*, Microwave frequency multiplication by hot electrons, // J. Appl. Phys. 1963. 34, 1608-1610.

20. *Nimtz G. and Seeger K.*, Microwave mixing by hot electrons in homogeneous semiconductors // J. Appl. Phys. 1968. 39, 2263-2266.

21. Mayer A. and Keilmann F., Far-infrared nonlinear optics. I. χ^2 near ionicresonance, // Phys. Rev. B. 1986. 33, 6954-6961.

22. Dekorsy T., Yakovlev V.A., Seidel W., Helm M., and Keimann F., Infrared phonon-polariton resonance of the nonlinear susceptibility in GaAs // Phys. Rev. Lett. 2003. 90, 055508-1/4.

23. McFee J.H., Boyd G.D., Schmidt P.H. Redetermination of the nonlinear optical coefficients of Te and GaAs by comparison with Ag3SbS3 // Appl. Phys. Lett. 1970. V.17 P.57.

24. Flytzanis C. Infrared Dispersion of Second-Order Electric Susceptibilities in Semiconducting Compounds // Phys.Rev. B. 1972. v.6, 1264.

25. *Madelung*, Semiconductors: Data Handbook (Springer-Verlag, New York, 2003).

26. *Akitt D., Johnson C., Coleman P.* Nonlinear susceptibility of CdTe // IEEE Journal of quantum electronics. 1970. V. QE - 6, 496.

27. Frits Zernike & John E. Midwinter Applied Nonlinear Optics John Wiley & Sons Inc. 1973

28. *Alyabyeva L.N., Zhukova E.S., Belkin M.A., and Gorshunov B.P.* Dielectric properties of semi-insulating Fe-doped InP in the terahertz spectral region // Scientific Reports. 2017. 7. 7360.

Molecular beam epitaxial growth of semiconductor heterostructures for THz electronics

Victor M. Ustinov[1,2]

[1]Ioffe institute, St. Petersburg, Russia, vmust@beam.ioffe.ru
[2]SHM R&E Center, RAS, St. Petersburg, Russia

In recent two decades semiconductor heterostructures emerged as a very promising basis for the development of various types of devices in a microwave frequency range. In the present work we discuss molecular beam epitaxial (MBE) growth of wide miniband superlattice (SL), heterostructure barrier varactor (HBV) and high electron mobility transistor (HEMT) structures, their characterization and application of these heterostructures for generators, detectors and frequency multipliers operating in the sub-THz and THz frequency range.

Superlattices.

The superlattice structures were grown by solid source molecular beam epitaxy using a Riber 32 machine. GaAs based structures were grown on GaAs substrates, consisted of several tens of periods of GaAs wells (3 - 4 nm thick) and AlAs barriers (about 1 nm thick) doped with silicon (10^{17} - 10^{18} cm^{-3}). The superlattice was embedded between graded layers of gradual composition and doping level to avoid abrupt heterojunctions. A n^+ GaAs or GaAs/InGaAs cap layer was provided for the formation of ohmic contacts. InP based SL structures were grown lattice matched to InP substrates and consisted of several tens of periods of $In_{0.53}Ga_{0.47}As$ wells (about 4 nm thick) and $In_{0.52}Ga_{0.48}As$ barriers (about 1.2 nm thick) doped with silicon (10^{17} - 10^{18} cm^{-3}). The superlattice was embedded between graded layers of gradual composition and doping level to avoid abrupt heterojunctions. InGaAs cap layer was provided for the formation of ohmic contacts. Mesa diodes (Fig. 1) with area of about 60 and 10000 μm^2 were formed using Au–Ge–Ni composition [1].

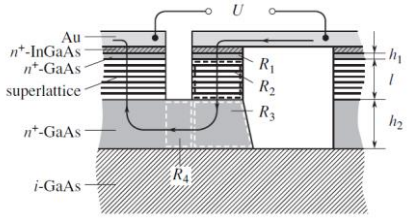

Fig. 1. Cross section of the GaAs based diode structure

Changing the widths of the well and barrier layers the lowest SL miniband width could be varied from about 20 up to 160 meV. These doped wide miniband superlattices exhibit negative differential conductance (NDC), Fig. 2, which is a consequence of Bragg reflection of miniband electrons accelerated by an electric field.

The negative differential mobility of a superlattice can give rise to travelling dipole domains and a self-sustained current oscillation at the transit frequency, which is the ratio of the domain velocity and the superlattice length. The fundamental oscillation frequency increased with the increase in the miniband width due to the increase of peak drift velocity [2]. The oscillation frequency can be controlled by changing the bias voltage applied to the diode. In comparison to a GaAs/AlAs superlattice, an InGaAs/InAlAs superlattice with the same quantum well and barrier thickness has the advantage of a larger miniband and, therefore, of a higher drift velocity due to the lower effective electron masses of the constituent materials and a lower barrier height. The highest fundamental frequency of an InGaAs/InAlAs superlattice oscillator is shown on Fig. 3. The power was ~80 mW corresponding to a conversion efficiency from DC to high-frequency power of 0.6% [3].

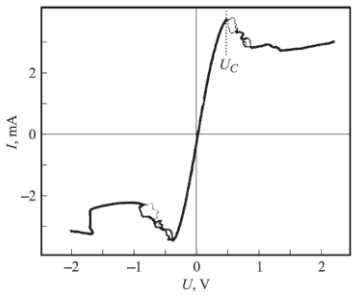

Fig. 2. Current-voltage characteristic of SL diode

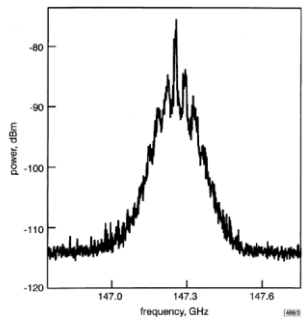

Fig. 3. Spectrum of millimetre wave emission from InGaAs/InAlAs superlattice device.

Strongly nonlinear U-V characteristic in the NDC region allows the use of the doped wide miniband superlattice device as a frequency multiplier in the microwave emission range, Fig. 4. The input frequency F = 150 GHz. Maximum harmonic number is n = 54, maximum harmonic frequency is 8.1 THz. Most part of radiation power of the frequency multiplier is concentrated in first 10 harmonics between 0.4 and 1.5 THz [4].

It was found that THz radiation affects Bloch oscillating miniband electrons. The direct current through a superlattice is reduced by a THz field and

resonant structures in the current–voltage characteristic occur when the Bloch frequency is in resonance

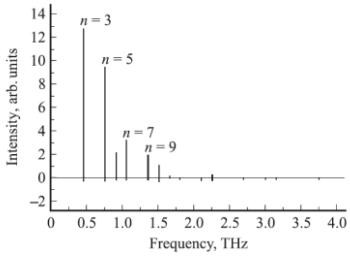

Fig. 4. GaAs/AlAs SL frequency multiplier harmonics intensity in the 0.4 – 4.1 THz range.

with the THz field or with its harmonics. In comparison to a GaAs/AlAs superlattice detector, the InGaAs/InAlAs superlattice detector has a responsivity, which is higher by an order of magnitude. The higher responsivity is caused by a higher current density due to a larger miniband of the InGaAs/InAlAs superlattice [5].

Heterostructure barrier varactors.

Heterostructure barrier varactor (HBV), Fig. 5, frequency multipliers demonstrate very promising results for applications in sub-THz and THz range. The best results for HBV multipliers have been achieved using MBE-grown heterostructures on InP substrates with several $In_{0.52}Al_{0.48}As/AlAs/In_{0.52}Al_{0.48}As$ barrier layers in the $In_{0.53}Ga_{0.47}As$ matrix. We have found that leakage current strongly decreases with the increase in the AlAs insertion thickness due to the reduction in the electron tunneling probability. Strain compensation InGaAs layers also decrease the leakage current at the same AlAs thickness. This may be attributed to the positive effect of the decrease in the overall amount of strain in the structure and better structure quality. Frequency tripler was fabricated using 6 mesa,18 barrier HBV diode, with a cross section area of 7x150 μm^2. Under CW operation at 94 GHz output frequency the maximal output power exceeds 100 mW at the conversion efficiency of about 14%. The estimated value of HBV cut-off frequency exceeds 1.2 THz [6].

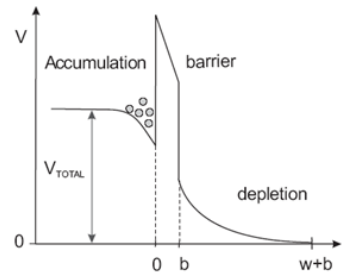

Fig. 5. HVB conduction band diagram at applied bias voltage.

HEMTs.

Nonlinear properties of the plasmonic excitations in a two-dimensional electron channel of HEMT can be used for detection of terahertz (THz) radiation. The plasmonic FET THz detectors are promising because they can operate in a broad THz frequency range at ambient temperature and exhibit a good balance between the responsivity and noise figure of merit. Along with the plasmonic nonlinearity, the asymmetry of the boundary conditions at the source and drain ends of the HEMT electron channel is mandatory for enabling a non-zero detection response. We fabricated a tight concatenation of four HEMT s connected in series on a single chip. It is shown that such HEMT chain exhibits strong THz photovoltaic response due to asymmetric form of the T-gate in each HEMT in the chain. We obtained the voltage responsivity above 1 kV/W in the unbiased mode of the detector operation [7].

References

1.*D. G. Pavel'ev, N. V. Demarina, Yu. I. Koshurinov, A. P. Vasil'ev, E. S. Semenova, A. E. Zhukov, V. M. Ustinov* Characteristics of planar diodes based on heavily doped GaAs/AlAs Superlattices in the terahertz frequency region // Semiconductors. 2004. V. 38, No. 9. P. 1105–1110.

2. *E. Schomburg, T. Blomeier, K. Hofbeck, J. Grenzer, S. Brandl, I. Lingott, A. A. Ignatov, K. F. Renk, D. G. Pavel'ev, Yu. Koschurinov, B. Ya. Melzer, V. M. Ustinov, S. V. Ivanov, A. Zhukov, P. S. Kop'ev* Current oscillation in superlattices with different miniband widths // PHYS. REV. B. 1998. V. 58, No. 7. P. 4035 – 4038.

3. *E. Schomburg, R. Scheuerer, S. Brandl, K.F. Renk, D.G. Pavel'ev, Yu. Koschurinov, V. Ustinov, A. Zhukov, A. Kovsh, P.S. Kop'ev* InGaAs/InAlAs superlattice oscillator at 147GHz // Electron. Lett. 1999. V. 35, No. 17. Online No: 19990973

4. *D. G. Paveliev, Y. I. Koshurinov, A. S. Ivanov, A. N. Panin, V. L. Vax, V. I. Gavrilenko, A. V. Antonov, V. M. Ustinov, A. E. Zhukov* Experimental study of frequency multipliers based on a GaAs/AlAs semiconductor superlattices in the terahertz frequency range // Semiconductors. 2012. V. 46, No. 1 P. 121–125.

5. *E. Schomburg, F. Klappenberger, M. Kratschmer, A. Vollnhals, R. Scheuerer, K.F. Renk, V. Ustinov, A. Zhukov, A. Kovsh* InGaAs/InAlAs superlattice detector for THz radiation // Physica E. 2002. V. 13, P. 912 – 915

6. *N. A. Maleev, V. A. Belyakov, A. P. Vasil'ev, M. A. Bobrov, S. A. Blokhin, M. M. Kulagina, A. G. Kuzmenkov, V. N. Nevedomskii, Yu. A. Guseva, S. N. Maleev, I. V. Ladenkov, E. L. Fefelova, A. G. Fefelov, V. M. Ustinov* Molecular-Beam Epitaxy of InGaAs/InAlAs/AlAs Structures for Heterobarrier Varactors // Semiconductors 2017. V. 51, No. 11. P. 1431–1434.

7. *V. V. Popov, D. M. Yermolaev, K. V. Maremyanin, V. E. Zemlyakov, N. A. Maleev, V. I. Gavrilenko, V. A. Bespalov, V. I. Yegorkin, V. M. Ustinov, S. Yu. Shapoval* Detection of terahertz radiation by tightly concatenated InGaAs field-effect transistors integrated on a single chip // Appl. Phys. Lett. 2014. V.104, 163508

Theoretical and experimental studies of dielectric two-dimensional Bragg structures for development of spatially-extended heterolasers

N.Yu. Peskov, V.R. Baryshev, N.S. Ginzburg, E.R. Kocharovskaya, A.M. Malkin, D.M. Padozhnikov, M.D. Proyavin and V.Yu. Zaslavsky

Institute of Applied Physics RAS, Nizhny Novgorod, Russia, peskov@appl.sci-nnov.ru

Introduction

Two-dimensional distributed feedback (2D DF) was originally proposed [1] for obtaining super-power coherent radiation in relativistic masers based on spatially-extended electron beams. In this case, the 2D DF mechanism is realized in a 2D-periodic metallic Bragg structures with doubly periodic corrugation, which due to the arising in them of the transverse wave-flaxes allow synchronization of radiation of wide electron beams and the establishment of a single-mode oscillation regime when their transverse dimensions are in orders of magnitude greater than the radiation wavelength. To date, the operability of the new feedback mechanism has been experimentally demonstrated in the FEMs, which were elaborated in the millimeter wavelength range (from Ka- up to W-bands) under a record transverse size of the interaction space, reaching up to 50 wavelengths, and the output power level of ~ 50 - 100 MW [2, 3].

At the same time, high potential of the new feedback mechanism is not exhausted by microwave relativistic generators. In this aspect it should be noted that currently a 1D feedback mechanism, which is realized in "traditional" single-periodical Bragg structures based on the coupling and mutual scattering of two counter-propagating waves, is widely used in quantum DF lasers [4, 5]. However, the transverse sizes of such generators in the conditions of maintaining single-mode narrow-band oscillation are limited by several wavelengths, and further enhance of dimensions leads to a complication of the radiation spectrum and, thus, loss of its spatial coherence. One of the attractive ways to solve this problem in heterolasers is the use of novel 2D feedback mechanism (Fig. 1), which in this case can be realized in 2D Bragg structures of planar geometry with double-periodical modulation of the effective refractive index

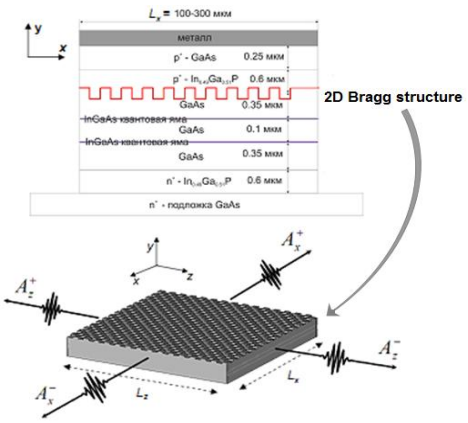

Fig. 1. Scheme of heterolaser based on 2D Bragg structure.

of the dielectric waveguide. According to the theoretical analysis carried out in [6], the use of these structures makes it possible to synchronize the radiation from the active medium characterized by large Fresnel parameters in both transverse directions.

The paper presents results of theoretical analysis and computer simulations of the electrodynamic properties of dielectric 2D Bragg structures of planar geometry. "Cold" tests of prototypes of the structures were carried out in the W-band and demonstrated good coincidence with the design parameters. Possibility to advance structures of this type in the sub-mm ranges is discussed.

Results of simulations and “cold” tests in W-band

One of the main issues of the study was the analysis of acceptable technologies for the manufacture of planar dielectric Bragg structures. For operation at mm wavelengths, the technology based on the 3D computer printing, which characterized by a high speed of production and affordable cost of the models, was developed.

An important aspect for the discussed technology is the study of dielectric properties of plastics used for printing (which are practically not available in the standard descriptions and strongly depend on the quality and printing characteristics). Complex dielectric permittivities of different plastics were tested using a network analyzer in the Ka- and W-bands by measuring the reflection and transmission coefficients through a standard waveguide having the inserts from these dielectrics. The values of dielectric permittivity (complex and imaginary parts) were found by comparing the measured characteristics with the calculated ones (using iterative procedure). As a result of the experiments were selected plastics, the most suitable for the manufacture of the structures. Measured value of the dielectric constant was $\mathrm{Re}\,\varepsilon = 2.4$ and $\tan\delta = 0.0015$. At the same time, the experiments did not identify strong frequency dependences of these coefficients in tested bands.

Simulations of planar dielectric 2D Bragg structures were performed using the commercial code CST "Microwave Studio". Parameters for the simulations were chosen similar to the conditions of the experiments described below. Results of simulations of the frequency dependences of the integral scattering coefficients on the 2D structure (reflection, transmission, and transverse scattering coefficients) are presented in Fig. 2. It is showed good agreement with the results of previous theoretical analysis carried out in [6]. In the designed region of parameters the effective Bragg

scattering zone corresponding to the coupling of the four partial wave-flaxes, which possess the structure of the TM-wave of the dielectric waveguide propagating over the corrugated surface, was verified.

Experimental study of 2D Bragg dielectric structures was conducted in the W-band. The thickness of the dielectric waveguide was 2 mm, the so-called "chessboard" corrugation was made on this waveguide with a period along each (x and z) directions $d_x = d_z = 4$ mm and a depth of 0.5 mm (Fig. 3). The transverse dimensions of the structure were 18 см × 18 см, the structure (dielectric waveguide) was placed on a substrate of duralumin.

A network analyzer P2-67 was used as the RF signal source. To form incident wave-beam (and receiving scattered radiation), the planar quasi-optical transmission line, which provides at its output a wide wave-beam with the structure of TEM-wave and plane phase, was exploited (Fig. 3). The results of "cold" measurements of the reflection and transmission coefficients on the structure described above are shown in Fig. 4. In accordance with the calculations, an effective Bragg scattering zone was observed in the vicinity of 60 GHz. Comparison Fig. 2 and 4 demonstrates good agreement between the simulations and "cold" tests results both on the position and width of the Bragg zone as well as on the amplitude of the integral scattering coefficients.

Summary and discussions

Thus, theoretical and experimental studies have confirmed the feasibility and operability of the 2D dielectric Bragg structures in the mm wavelength band. The available technology of manufacturing structures of this type using the 3D printing was developed. The good coincidence of the electrodynamic properties of the 2D structures measured in "cold" tests with the results of computer simulations based on commercial code CST "Microwave Studio" was demonstrated. The experimental studies have confirmed that the dielectric properties of plastics utilized in the proposed technology are adequate for manufacturing models of dielectric 2D structures with the accuracy acceptable for operation up to a short-wave part of the mm wavelength band. The further development of the 2D Bragg structures of the discussed type should be directed to advance into the sub-mm range when using the industrial 3D printers and the polymer photo printing technology, the claimed accuracy of which currently reaches up to 1 μm.

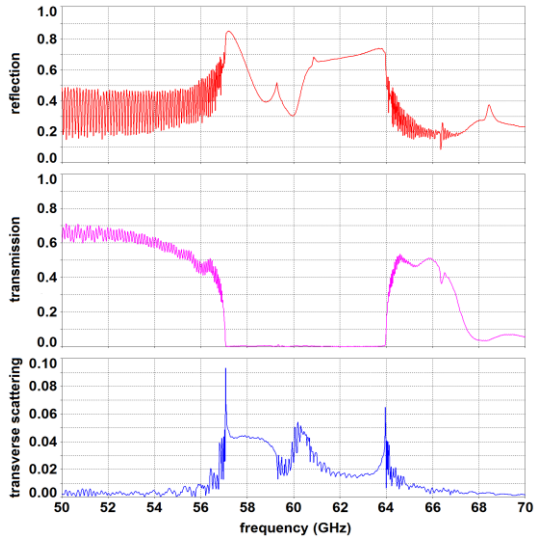

Fig. 2. Results of CST - simulations of dielectric 2D Bragg structure having parameters close to experimental prototype. Frequency dependencies of the reflection (top), transmission (middle) and transverse scattering (bottom) coefficients.

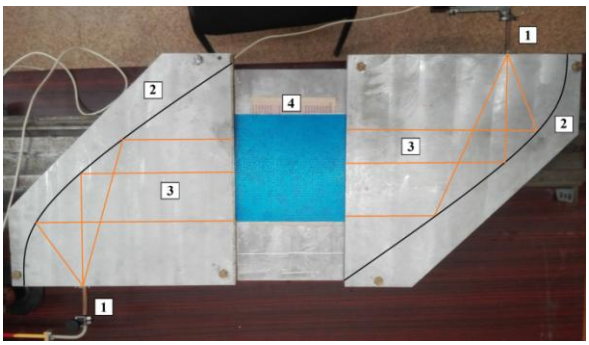

Fig. 3. Scheme of the "cold" tests: 1 - standard single-mode waveguides powered by the network analyzer, 2 - planar quasi-optical transmission lines, 3 - incident and transmitted wave-beams, 4 - dielectric 2D Bragg structure.

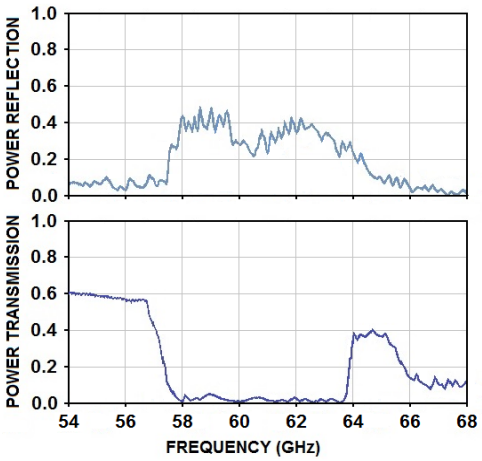

Fig. 4. Results of "cold" measurements of frequency dependencies of the reflection (top) and transmission (bottom) coefficients of dielectric 2D Bragg structure in the W-band.

This work is partially supported by the Russian Foundation for Basic Research (grant 18-48-520022).

References

1. *N.S.Ginzburg, N.Yu.Peskov, A.S.Sergeev*. Dynamics of free-electron lasers with two-dimension distributed feedback // Optics Commun. 1994. V.112. P.151.
2. *N.S.Ginzburg, N.Yu.Peskov, A.S.Sergeev, e.a.* Production of powerful spatially coherent radiation in planar and coaxial FEM exploiting two-dimensional distributed feedback // IEEE Trans. on Plasma Sci. 2009. V.37. No.9. P.1792.
3. *A.V.Arzhannikov, N.S.Ginzburg, P.V.Kalinin, e.a.* Using two-dimensional distributed feedback for synchronization of radiation from two parallel-sheet electron beams in a Free-Electron Maser // Phys. Rev. Lett. 2016. V.117. P.114801.
4. *H.Kogelnik, C.V.Shank.* Stimulated emission in a periodic structure // Appl. Phys. Lett. 1971. V.18, No.4. P.152.
5. *A.Yariv*. Quantum Electronics // John Wiley and Sons Inc., New York, 1975.
6. *N.S.Ginzburg, V.R.Baryshev, A.S.Sergeev, A.M.Malkin*. Dynamics of semiconductor lasers with two-dimensional distributed feedback // Phys. Rev. A. 2015. V.91. P.053806.